SLOVAK UNIVESITY OF TECHNOLOGY IN BRATISLAVA
Faculty of Electrical Engineering and Information Technology

Ing. Stanislava Serečunová

Dissertation Thesis Abstract

DESIGN, SIMULATION AND OPTIMIZATION OF PASSIVE PHOTONIC DEVICES FOR COMMUNICATION AND MEDICAL APPLICATIONS

to obtain the Academic Title of abbreviated as (philosophiae„PhD.“)

in the doctorate degree study programme: Electronics and Photonics
in the field of study: Electrical and Electronics Engineering
in form of study: Part-time study

Place and Date: Bratislava, September 2023

Dissertation Thesis has been prepared at the Institute of Electronics and Photonics, Faculty of Electrical Engineering and Information Technology, Slovak University of Technology in Bratislava

Submitter: Ing. Stanislava Serečunová
Faculty of Electrical Engineering and Information Technology
Electronics and Photonics
Ilkovičova 3, 841 04 Bratislava

Supervisor: prof. Ing. František Uherek, PhD.
Faculty of Electrical Engineering and Information Technology
Electronics and Photonics
Ilkovičova 3, 841 04 Bratislava

Consultant: Dr. habil. Dana Seyringer, PhD.
Vorarlberg University of Applied Sciences
Research Centre Microtechnology
Hochschulstraße 1, 6850 Dornbirn

Readers: Erich Leitgeb, Ao.Univ.-Prof. Dipl.-Ing. Dr.techn.
Graz University of Technology
Institut für Hochfrequenztechnik
Inffeldgasse 12/I, 8010 Graz

doc. Ing. Jozef Novák, DrSc.
Institute of Electrical Engineering
Slovak Academy of Sciences
Dúbravská cesta 9, 841 04 Bratislava

Dissertation Thesis Abstract was sent: .....

Dissertation Thesis Defence will be held on..... **at**.....
at Faculty of Electrical Engineering and Information Technology, Slovak University of Technology in Bratislava, Ilkovičova 3, 81219 Bratislava

.....
prof. Ing. Vladimír Kutiš, PhD.
(Dean of Faculty)

Contents

Introduction

Optics and photonics technologies impact nearly all areas of our lives and cover a wide range of applications in science and industry, including information and communication technology, production, medicine and life science engineering, as well as in energy and environmental technology.

Nowadays, communication systems using metal lines are being replaced by optical communication systems. Metallic lines are reaching their limits in terms of transmission bandwidth while the requirements of participants are increasing. Therefore, the data is increasingly being transmitted using optical signals over optical fibers. Telecommunication optical systems can use wavelengths around an operating wavelength of 850 nm, the so-called first telecommunications window. Systems using the first telecommunications window are designed for less demanding data transmission, both economically and technically, over shorter distances with lower data volumes. Core networks use an operating wavelength around 1310 nm, the so-called second telecommunications window, where the silica optical fibers have the lowest dispersion. the wavelengths around the operating wavelength of 1550 nm, the so-called third telecommunications window, are used for long-haul optical data transmission, where the silica fibers have the lowest optical losses [1].

The passive optical splitters focused on the telecommunication industry are one of the key components in passive optical networks, particularly in Fiber-To-The-Home technology. This technology enables high-speed broadband connections simultaneously to multiple users at home, businesses, or other locations, depending on where the optical fiber is terminated. the task of the splitters is to split one optical signal into many identical signals bringing, for instance, the same TV signal to different households. the more buildings can be served by one optical splitter, the lower the installation costs are [2, 3].

The applicability of new data-transmitting technologies and various materials gives great potential in new industrial technologies as well as in telecommunications. For instance, polymer materials are becoming more and more promising and are looking for a solid place in the field of photonics and biophotonics. Their use in this area allows better integration of various components on the chip. Modern treatments in photonics based on polymer technologies offer the implementation and integration of the interconnects in a three-dimensional configuration based on a three-dimensional laser lithography fabrication process. Some potential applications include routing for

next-generation intra-chip optical communication and parallel photonic neural networks [4].

Minimizing the structure of passive optical components is desirable to achieve more compact functional integrated optical circuits with reduced propagation and scattering losses. Silicon nitride photonics has become increasingly common for advanced photonics devices that demand higher performance than traditional silica waveguides. Waveguides based on the silicon nitride material platform are fully complementary metal-oxide semiconductor-compatible, offer wide wavelength transparency and feature lower optical propagation losses than major silicon photonics platforms and indium phosphide [5]. They open the ability to carry wavelengths over a wider range, not only in 'traditional' wavelength ranges used for telecommunication applications (1250 - 1350 nm, 1520 - 1660 nm) but also in the visible (450 - 750 nm) and a distinct part of the near-infrared spectrum (750 - 1000 nm). For instance, analytical and diagnostic systems in the life sciences rely on visible light for sensing and imaging. By introducing integrated photonics technology, the size of devices can be reduced, resulting in compact handhelds [6].

The dissertation thesis aims to design, simulate and optimize passive optical components for telecommunication and medical applications. According to the analysis of the optical properties such as insertion loss, non-uniformity, or background crosstalk, the goal was to improve the performance and functionality and also to reduce the size and cost of the designed passive optical components. Finally, the selected splitter designs were fabricated and their functionality was verified.

Objectives of the dissertation thesis

1. Obtaining the knowledge of the principle of passive optical components and their use in telecommunication and medical applications.
2. Design, simulation and optimization of optical splitters based on the Y-branching and multimode interference approach for telecommunication applications based on silica-on-silicon material platform.
3. Design, simulation and optimization of two dimensional and three dimensional optical splitters for telecommunication applications based on polymers.
4. Design, simulation, and optimization of selected passive optical components for integration on chip based on SiN.

1. Brief state-of-the-art

Low-index-contrast (SiO_2-based, silica-on-silicon, SoS) waveguide devices still hold a large market share because of their many advantages. First, their modal field matches well with that of single-mode optical fibers, making it relatively easy to couple them to fibers. Second, they combine low propagation loss (<0.05 dB/cm, because there is little absorption and scattering in the waveguides) with high fiber-coupling efficiency (low losses on the order of 0.1 dB) [7]. Therefore, they are more mainly used in telecommunication applications. However, the very low refractive-index contrast means the bending radius of the waveguides needs to be very large (order of several millimeters) and may not fall below a particular critical value to suppress bending losses. As a result, silica-based waveguide devices usually have a very large size that limits the integration density of SiO_2-based photonic integrated devices.

Advancements in polymer technologies offer the implementation and integration of photonics interconnects in 3D configuration. Especially, the modern treatments based on the two-photon polymerization (2PP) lithography fabrication process rapidly accelerated the freestyled designs in 3D photonic devices and structures. The 2PP lithography has simplified many complex fabrication steps, enabling designers to directly print from a digital model and flexibly design and attach arbitrary optical components using more straightforward alignment techniques [8]. The 3D splitters for interconnects are an important technological asset, for instance, for next-generation optical routing, on and intra-chip optical communication, and for parallel photonic neural networks [4].

In recent years, the splitters and other passive optical components have found applications in various medical and biomedical fields, also in applications for miniaturization on a chip. They use silicon nitride (Si_3N_4) material for photonic integrated circuits (PICs), which is an alternative to high-index contrast silicon-on-insulator (SOI) and low-index contrast SoS material platforms, having a moderate index contrast lying between both main groups [9]. This amorphous material is more thermodynamically stable and compatible with CMOS technology. The lower refractive index contrast makes it more resistant to fabrication imperfections and surface roughness in waveguide structures, resulting in a lower signal loss in transmission. In addition, it provides the possibility of monolithic cointegration with silicon photodiodes and electronic circuits based on CMOS technology [5]. Si_3N_4-based passive optical components can be applied to the on-chip implementation of a wide range of applications, such as optical biosensors [10], beam steering devices [11], or optical spectrometers for near-infrared spectroscopy [12]. They can

be used in PIC-based biosensing applications to measure different physical or biochemical parameters. In most cases, the optical radiation must be guided through the analyte. For instance, integrating splitting devices with suitable sensing elements, such as microfluidic devices, can detect and separate airborne inorganic particles for pollution monitoring [13]. The other intriguing options for analyzing many biomarkers enable label-free detection [14]. Splitters can be applied in miniaturized and portable diagnostic systems for point-of-care applications based on flow cytometry [15, 16] or environmental monitoring [17, 13].

2. Silica-based components for telecommunication applications

This chapter presents the design, simulation and optimization of Y-branch splitters with up to 128 output waveguides and the high splitting ratio multimode interference (MMI) splitter with 128 output waveguides. The aim is to find the minimum physical dimensions of the designed splitters with satisfactory optical performance. According to the minimum insertion loss IL and minimum non-uniformity ILu, the optimum length, shape and size of the spitters are determined. The design, simulation and optimization of the splitters are performed by a commercial photonics software tool - OptiBPM from Optiwave, which uses the beam propagation method.

2.1 Material platform

The optical waveguide structure, used in the designs of every optical splitter, is a silica-on-silicon buried rectangular channel. The proposed optical splitters were designed and simulated for the telecommunication operating wavelength, $\lambda = 1550$ nm. For this operating wavelength, a core layer with a refractive index $n_c = 1.456$ is used, which is transversely surrounded by a cladding layer having a refractive index $n_{cl} = 1.445$. The refractive-index contrast between the cladding and the core is $\Delta n = 0.75$ %. These refractive indices were taken from a professional technological partner. The waveguides were set to have a core size (6×6) µm^2, which is a standard size used in passive optical waveguide components for telecommunication applications [18, 19]. A guided optical wave then propagates along with its longitudinal direction in the waveguide.

2.2 1×2^N Y-branch splitters

A conventional Y-branch splitter structure consists of an input waveguide $L(in)$, splitting waveguides $L(n)$, and output waveguides $L(out)$, as presented in Fig. 2.1. The input waveguide $L(in)$ is required to link the optical signal from the optical fiber into the splitter, and the output waveguides $L(out)$ are used to stabilize the intensity profile. Both were set to have a length of $L(in) = L(out) = 500$ µm. The waveguides placed between the input/output waveguides $L(n)$ were used to split the optical signal.

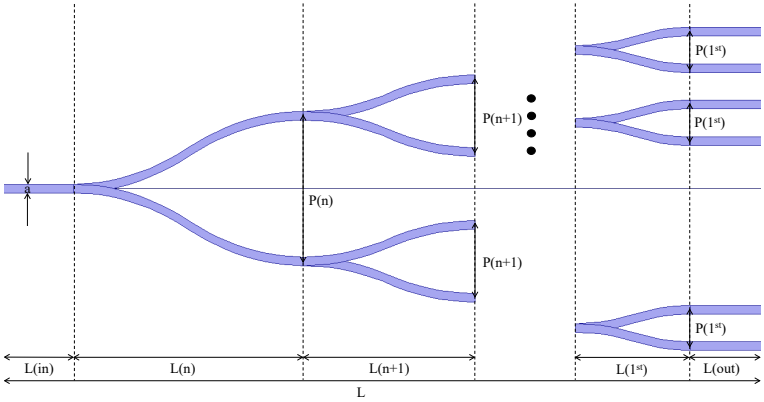

Figure 2.1: Schematic view of the proposed 1×2^N Y-branch splitters [20].

Each individual Y-branch is constructed of two waveguides with a predefined cosine arc S-shape called Arc S-Bend. Based on the Y-branch geometry, which has been explored in [21, 22], this shape is supposed to provide the least losses. The space between the ending of two S-Bend branches is called a port pitch P. The port pitch $P(1^{st})$ between the all output waveguides $L(out)$ is set to 127 µm. This spacing is required for a connection with fibers [23]. This initial port pitch value is then doubled with every further layer $L(n+1)$ towards the input waveguide $L(in)$. For instance, the 1×4 Y-branch splitter structure contains one Y-branch with a 245 µm port pitch and two Y-branches with a 127 µm port pitch. Such a cascade arrangement allows the splitting of one input optical signal into four output optical signals [24].

This approach is used to design and optimize further split ratios 1:8, 1:16, 1:32, 1:64, and even more complex splitting structures, like 1×128 Y-branch optical splitters.

The goal of this thesis objective was to design the Y-branch splitters up to a 128-splitting ratio with a small footprint and good optical properties. Therefore it was first necessary to define the 1×2 Y-branch waveguides for the length $L(1^{st})$ and port pitch $P(1^{st})$. Then the splitter had the seven branching layers, and if they were joined together in the cascaded system, the splitter reached a 1×128 splitting.

Figure 2.2 shows the design of the final length-optimized 1×128 Y-branch splitter with an Arc S-Bend waveguide shape [20].

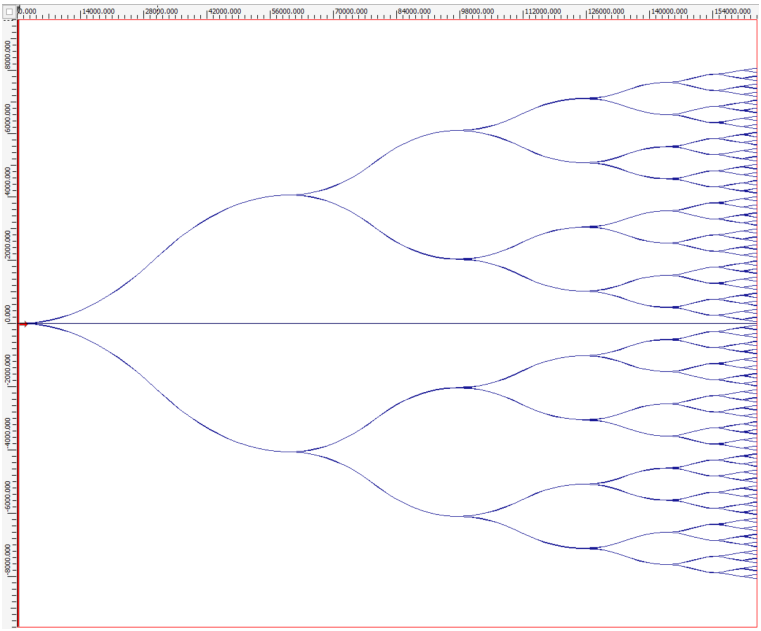

Figure 2.2: Design of 1 × 128 Y-branch optical splitter with Arc S-Bend waveguide shape [20].

2.2.1 Optimization

The optimization of Y-branch splitters represents an important post-design step, which aims to achieve minimum dimensions without worsening their optical properties. The optimization of these Y-branch splitters consisted of several steps:

- each Y-branch length, consisting of S-Bend waveguides, was optimized,
- the waveguide core size was reduced and the length of Y-branches was optimized for the new waveguide core size,
- to suppress the optical radiation scattering from the waveguides, all S-Bend waveguide shapes (Arc, Sine, Cosine) were applied and studied,
- the S-Bend waveguide shapes were applied to Y-branch splitters with optimized waveguide core size,
- a supporting script for automated evaluation of optical properties (IL, ILu, BX) was developed for evaluating the splitters with high splitting ratios.

2.2.2 Final results

The Y-branch splitters were optimized based on the length of the individual splitting waveguides. Further, the splitters were optimized by reducing the waveguide core size from the standard (6×6) µm^2 to (5.5×5.5) µm^2 and further to (5×5) µm^2 to suppress the first mode in the used waveguides causing the unequal splitting. With each change in the waveguide core size, the Y-branch splitters were re-optimized for the length. The core resizing was applied to the splitters with all three S-Bend types: Arc, Cosine, and Sine.

Figure 2.3 shows the results of the optical properties of the highest

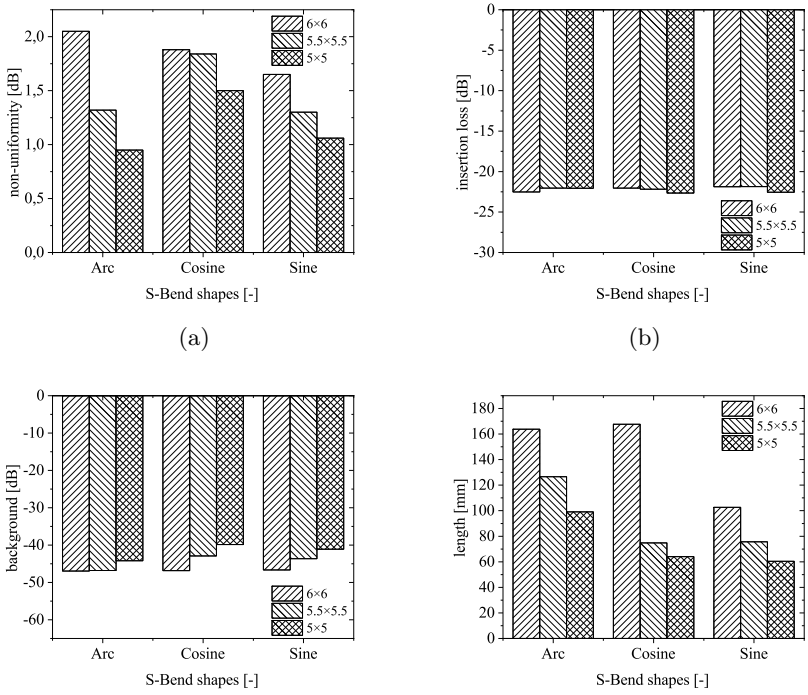

Figure 2.3: Comparison of 1×128 Y-branch splitter parameters for different waveguide core sizes applied for different S-Bend shapes: (a) non-uniformity (ILu), (b) insertion losses (IL), (c) background crosstalk (BX), (d) length of the splitters (L) [20].

reached Y-branch splitters with a splitting ratio of 1:128 for all S-Bend types, along with the reduction of the waveguide core size. Figure 4.6a shows how the non-uniformity ILu was improved by applying various S-Bend shapes when the waveguide core size was reduced. As can be seen, the most noticeable improvement occurred in the case of the Arc S-Bend shape, where the non-uniformity of 1×128 Y-branch splitter was suppressed to more than half of its original value (from 2.05 dB to 0.95 dB).

Figure 4.6b shows the calculated insertion loss IL at the end of the simulations. For all S-Bend waveguide shapes, the insertion loss of the splitters did not improve significantly with the reduction of the waveguide core size. Therefore, the small diversity of final values of the insertion loss can be neglected.

Background crosstalk BX is shown in Figure 4.6c. This value is the only one that has worsened when optimizing the waveguide core size of the 1×128 Y-branch splitters. In the case of the Arc S-Bend shape, it remained almost the same applying the waveguide core size (5.5×5.5) µm^2, and the background value, BX of the splitter with a waveguide core size (5×5) µm^2 deteriorated slightly. In the case of the Cosine and Sine S-Bend shapes, the background crosstalk values worsened with both waveguide core size reductions.

Significant improvement in the length of the 1×128 Y-branch splitter by decreasing waveguide core size is shown in Fig. 2.3d. In the case of Arc and Sine S-Bend waveguide shapes, the splitter length decreased linearly with decreasing waveguide core size (about one-third). In the case of Cosine S-Bend waveguide shape, the length of the splitter shortened dramatically to less than half when optimizing the waveguide core size from (6×6) µm^2 to (5.5×5.5) µm^2. The further reduction did not have such a significant influence on the splitter length.

The numerical results of the 1×128 Y-branch splitter simulations for all S-Bend types, together with the optimization of waveguide core size, are shown in Table 2.1. When considering only the length optimization (see column "Footprint"), the Y-branch splitter achieved the best results with a (5×5) µm^2 waveguide core size and Sine S-Bend shape, which reached 60400 µm. However, if all optical properties of the splitters were considered independently on the length (see columns "ILu", "IL" and "BX" in Tab. 2.1), one of the best results was achieved for the Y-branch splitter having a (5×5) µm^2 waveguide core size and Arc S-Bend shape. Considering both, the footprint and the performance optimization, the splitter with Sine S-Bend waveguide shape and waveguide cross-section size of (5.5×5.5) µm^2 had reached superior results.

Table 2.1: Summary of the optical properties of 1×128 Y-branch splitters with Arc, Cosine, Sine S-Bend waveguide shapes and waveguide core sizes (6×6) µm^2, (5.5×5.5) µm^2, and (5×5) µm^2.

S-Bend shape	Core size [µm^2]	ILu [dB]	IL [dB]	BX [dB]	Footprint [µm^2]
Arc	6×6	2.05	-22.51	-46.95	163800×16129
	5.5×5.5	1.31	-22.05	-46.79	126600×16129
	5×5	0.95	-22.06	-44.18	99100×16129
Cosine	6×6	1.88	-22.05	-46.83	167700×16129
	5.5×5.5	1.84	-22.17	-42.92	74800×16129
	5×5	1.50	-22.65	-39.84	64000×16129
Sine	6×6	1.65	-21.87	-46.65	102600×16129
	5.5×5.5	1.30	-21.86	-43.65	75700×16129
	5×5	1.06	-22.55	-41.11	60400×16129

2.3 1×128 multimode interference splitter

The MMI splitter designs with a higher splitting ratio do not depend on those with a lower splitting ratio, i.e., for every splitting ratio, the new MMI coupler parameters need to be defined. Therefore only the MMI splitter with the highest splitting ratio of 1:128 is presented. Figure 2.4 shows the geometry of the 1×128 multimode interference power splitter. The MMI splitter consists of an input waveguide $L(in)$, an MMI coupler L_{MMI}, tapers L_T, and branching output waveguides L_0^{MMI}. The input waveguide length $L(in)$ was set the same as for the Y-branch splitter, i.e., $L(in) = 500$ µm. The used waveguide material platform was the same as for Y-branch splitters, i.e., $n_c = 1.456$ and $n_{cl} = 1.445$ and the waveguide core size was (6×6) µm^2.

To design a multimode coupler, it is essential first to set the width of the coupler W_{MMI}. The broader the width, the longer the length of the resulting coupler will be. The 600 – 2000 µm range was chosen for testing the coupler width and the one with the best performance was selected. In this case, the width of the MMI coupler was set to $W_{MMI} = 1800$ µm. After the width of the MMI coupler is fixed, the length of the coupler L_{MMI} can be calculated approximately by [26]

$$L_{MMI} = \frac{n_c W_{MMI}^2}{N\lambda}, \tag{2.1}$$

where n_c is refractive index of the waveguide core, W_{MMI} is the width of

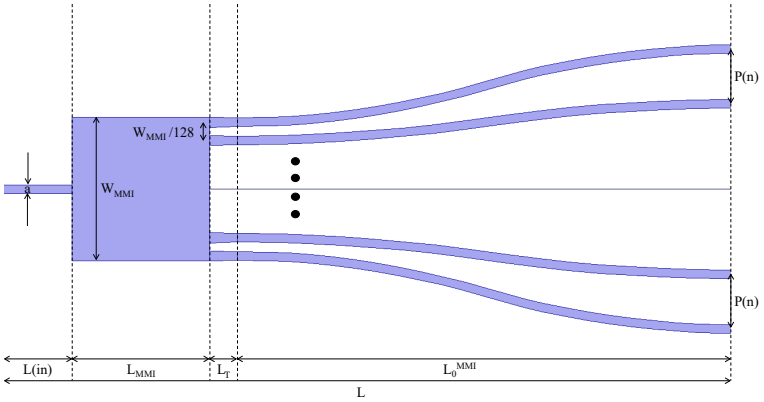

Figure 2.4: Schematic view of the proposed MMI splitter [25].

the MMI coupler, N is the number of output ports and λ is operating wavelength. From the calculation, the approximate length of the coupler reached $L_{MMI} = 23778$ µm. In the simulations, the length was optimized to 23832 µm to reach better optical properties of the splitter.

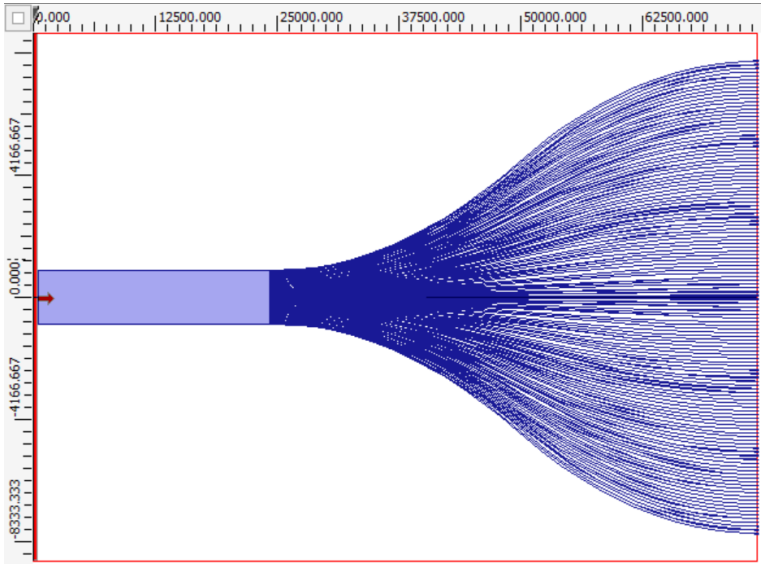

Figure 2.5: Design of 1 × 128 MMI optical splitter [25].

As a next step, the coupler was joined with 128 linear tapers L_T to stabilize the intensity profile. The length and input width of the tapers was tested to collect the maximum intensity from the MMI coupler into output waveguides. The separation between the tapers was $W_{MMI}/128 = 14.265$ µm and the input width of the taper was set to 9 µm. The output width of the linear tapers was kept at 6 µm, corresponding to the width of the waveguide. The length of the tapers was set to $L_T = 90$ µm and the length of the output branching waveguides $L_0^{MMI} = 50000$ µm. Finally, the port pitch between the output waveguides $P(n)$ was again set to 127 µm. Figure 2.5 shows the design of the final length-optimized 1 × 128 MMI splitter with the output waveguides having the Arc S-Bend shape [25].

Table 2.2 shows the simulation results of the 1 × 128 MMI splitter for both polarizations. The MMI splitters were evaluated for the same three optical parameters: non-uniformity ILu, insertion loss IL, and background crosstalk BX. As can be seen, the optical properties of the MMI splitter between TE and TM polarization are, in this case, very similar. The difference between non-uniformities is $\Delta ILu = 0.07$ dB and the difference between insertion losses are similar, only ΔIL = -0.06 dB and background crosstalk differ just by ΔBX = -0.40 dB. The results confirmed that the MMI splitter based on a silica-on silicon material platform is less polarization-dependent. The final size of 1 × 128 MMI splitter reached (74422 × 16129) µm^2.

Table 2.2: Results of 1 ×128 MMI splitter for both polarizations.

Polarization	Non-uniformity, ILu [dB]	Insertion loss, IL [dB]	Background crosstalk, BX [dB]	Footprint [µm^2]
TE	0.94	-21.80	-42.41	74422 × 16129
TM	1.01	-21.86	-42.01	

3. Polymer-based components for telecommunication applications

This chapter presents the design, simulation and optimization of 3D 1 × 4 MMI splitters with S-Bend output waveguides for fabrication by 3D lithography. Additionally, the design, simulation and fabrication of a novel 3D rectangular structure of 1 × 6 MMI coupler with direct integration to the end facet of standard single-mode optical fiber is presented.

3.1 Material platform

The optical waveguide structure used for designing the optical splitter is a polymer-based buried rectangular channel waveguide. The optical splitters described in this chapter were designed for the telecommunication operating wavelength, $\lambda = 1550$ nm. For this operating wavelength the core of the waveguide structure is IP-Dip polymer having $n_c = 1.53$, surrounded by a cladding layer of polydimethylsiloxane (PDMS) Sylgrad 184 with the refractive index of $n_{cl} = 1.3997$. The refractive index contrast is 8.52 %. The polymer IP-Dip is the most used photoresist employed for rapidly prototyping optical components. The cross-section of the waveguide was set to (2 × 2) µm^2 to reach the single-mode propagation only [27].

3.2 3D 1×4 multimode interference splitter

Based on the previous 2D design of the 1 × 4 MMI splitter [28], the following work was focused on a 3D arrangement of 2D 1 × 4 MMI splitter. Because the OptiBPM tool by Optiwave does not allow the splitter design in 3D space, this design was performed only in the BeamPROP simulation engine tool by RSoft Photonic Suite. Figure 3.1a shows the 3D 1 × 4 multimode interference splitter design schematic. The MMI splitter consists of an input waveguide, MMI coupler, and branching output waveguides. The length of the input waveguide $L(in)$ and the width W_{MMI} of the MMI coupler was taken from the design of the two-dimensional MMI structure [28]. The length of the input waveguide $L(in)$ was set to 10 µm. As already mentioned, to design a multimode coupler, it is important first to set the width of the coupler W_{MMI}. The same applies also to the length of the 3D MMI coupler. The MMI coupler cross-section was set to a square array of $W_{MMI} = (25 \times 25)$ µm^2. For this MMI coupler cross-section, the length L_{MMI} was optimized to 320 µm in the simulations to get better optical properties of the MMI coupler [29].

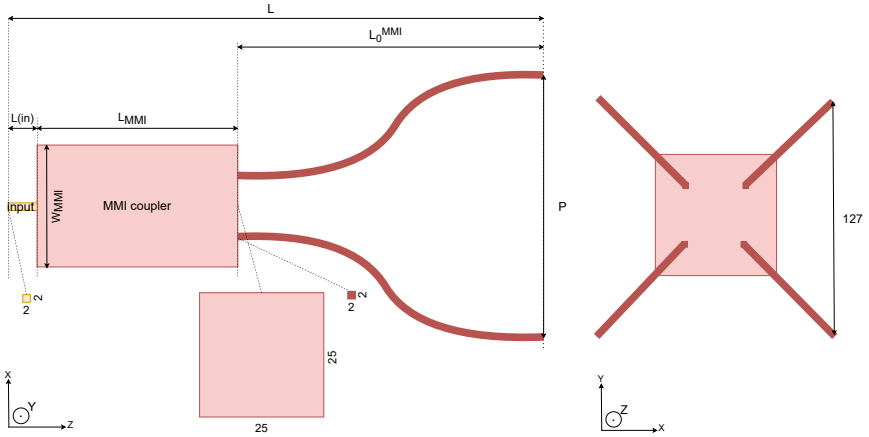

(a) (b)

Figure 3.1: Schematic view of 3D 1 × 4 MMI splitter: (a) side view, (b) positioning of the output waveguides.

As a following step, the output branching waveguides were joined to the end of the MMI coupler, and the positioning of the S-Bend output waveguides is shown in Fig. 3.1b. The length of the output waveguides was taken from the 3D 1 × 4 structure presented in [30, 27], which uses the Y-branch splitting principle. In the BeamPROP tool, pre-defined S-Bend waveguide shapes, Arc, Sine, and Cosine, were tested and the results showed that there was a minimum difference in the insertion losses between them. Therefore, it was continued with the pre-defined Arc S-Bend type. The length of the Arc S-Bend branches was set to 270 µm, as it was optimized for 3D 1 × 4 Y-branch splitter in [30, 27]. The upper arm of each Arc S-Bend offset was set to 63.5 µm, ensuring a required port pitch $P = 127$ µm [29].

3.2.1 Optimization

The structure of the 3D MMI splitter was optimized for the following parameters:

- the length of the output branches was scanned, and the optical properties were studied,
- the waveguide core size was optimized to improve optical properties,
- changing the material cladding layer was necessary because it was very challenging to use PDMS material as a cladding layer,

- the linear input waveguide was added to fit into single-mode fiber (SMF), and the cross-section width of the MMI coupler was further optimized,
- the linear output between the MMI coupler and S-Bend output waveguide and the positioning of the S-Bend output waveguides was also optimized.

3.2.2 Final results

Figure 3.2 shows the planar geometry of material optimized 3D 1 × 4 multimode interference power splitter. The single-mode fiber with a diameter of 10 µm had to be connected to the input linear waveguide. Therefore, the input part for SMF coupling is gradually linear tapered from cross-section (10 × 10) µm^2 to (4 × 4) µm^2 at the input to the MMI coupler of squared profile to reduce coupling losses. The length of the linear input taper was tested in the range of 20 - 80 µm and optimized to $L_T(in) = 40$ µm. Because the cladding layer was changed, the MMI coupler had to be optimized again. Therefore, the MMI coupler cross-section shrank to $W_{MMI} = (16 \times 16)$ µm^2, and its length was determined to be $L_{MMI} = 129$ µm.

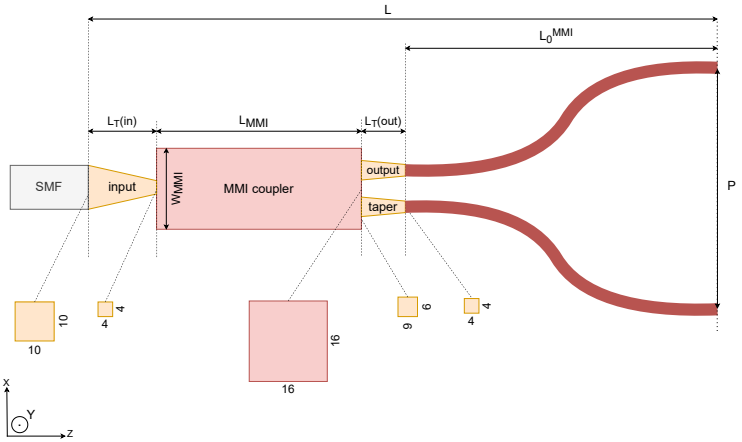

Figure 3.2: Schematic side view of material-optimized 3D 1 × 4 MMI splitter.

Due to the fabrication limit of 300 µm in one step, the fabrication had to be divided into two single-step processes. In the first step, the structure was fabricated till the end of the MMI coupler. However, since the exact positions of the output maxima at the end of the (16 × 16) µm^2 MMI coupler

were unknown, it was necessary to connect output tapers to the MMI coupler. The tapers are an essential part of the splitter structure for the correct connection of S-Bend output waveguides at intensity maxima to avoid significant losses. The linear output tapers were spaced equally apart at the end of the MMI coupler, with a cross-section of (6×6) µm^2 at the taper origin and (4×4) µm^2 at the exit (shown in Fig. 3.2). The taper length was optimized for maximum intensity at $L_T(out) = 20$ µm. The four S-Bend output waveguides were joined to the linear tapers with an Arc shape and had an $L_0^{MMI} = 270$ µm length. The radius of the Arc S-Bend waveguide was 321.18 µm, and the angle was 24.86 degrees. The port pitch between the S-Bend output waveguides was set to $P = 127$ µm for fiber connection. The final splitter structure consists of an SMF input, a tapered input waveguide, an MMI coupler (splitting part), linear output tapers and four S-Bend output waveguides with a total length of 459 µm [31, 32].

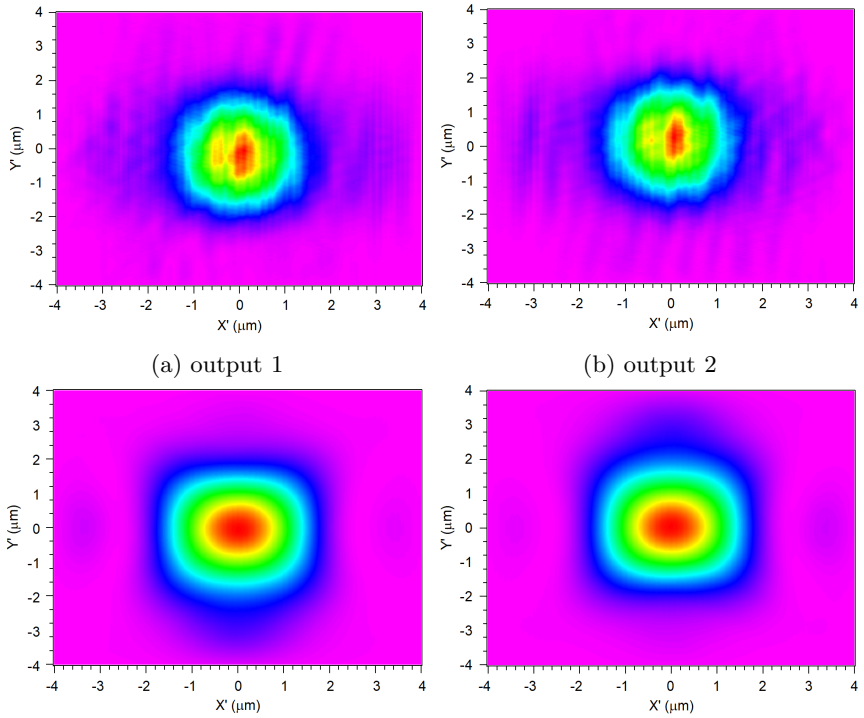

(a) output 1

(b) output 2

(c) output 3

(d) output 4

Figure 3.3: Simulated intensity distribution at the end of each S-Bend output waveguide [31].

The simulated optical power distribution of the optimized 3D 1 × 4 MMI splitter at the end of each S-Bend output waveguide is shown in Fig. 3.3. The insertion loss IL of the simulated 3D 1 × 4 MMI splitter was IL = -10.027 dB, with non-uniformity of the output signal distribution of ILu = 0.098 dB [31]. In spite of the fact that the insertion loss IL increased by approximately 2.3 dB and the non-uniformity ILu of the output signals also increased by 0.09 dB, compared to the previous 3D 1 × 4 MMI splitter structure with cladding layer PDMS, this structure could be fabricated.

3.2.3 Supporting structure design

After the designed 3D 1 × 4 MMI splitter was fabricated (see Fig. 3.4a), the structure was very fragile and lacked sufficient mechanical resistance. Therefore, an additional supporting mechanical structure was developed to enhance the mechanical stability of the splitter (see Fig. 3.4b). The SMF input port consists of four clamshells with sufficient flexibility to provide guidance and attachment to the SMF [31].

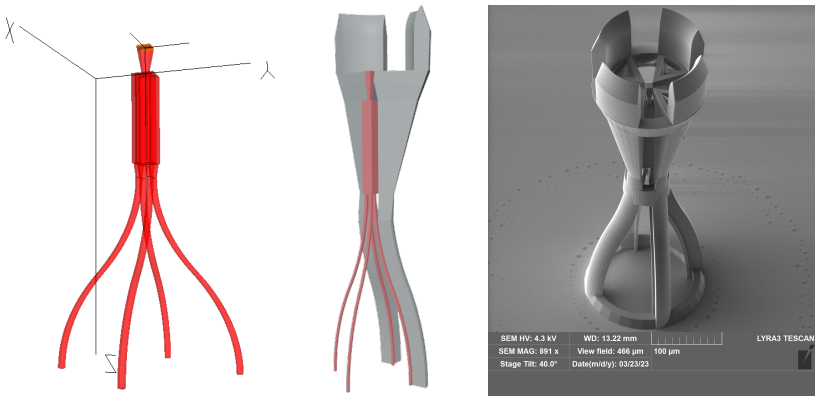

(a) (b) (c)

Figure 3.4: (a) Design of 3D 1 × 4 MMI splitter in RSoft tool, (b) partly revealed supporting mechanical structure (gray) for 3D 1 × 4 MMI splitter (red), (c) SEM image of the fabricated 3D 1 × 4 MMI splitter with a supporting mechanical construction.

3.2.4 Fabrication

In collaboration with the Department of Optics and Photonics at the University of Žilina [33], the designed 3D 1 × 4 MMI splitter structure was fabricated

in two single steps due to the length limitations of 300 µm in the fabrication process. In the first step, the structure up to 189 µm length was fabricated, i.e., till the end of the tapered linear outputs $L_T(out)$. In the second step, S-Bend outputs with a length of 270 µm were fabricated. The S-Bend outputs were mounted on the end of the linear tapers in a mechanical clamp that holds them in place. The Nanoscribe Photonic Professional GT was employed to fabricate the structure using a single-step direct laser writing system (DLW) based on two-photon polymerization (2PP) process. It used an Er-doped femtosecond frequency-doubled fiber laser that emits pulses at 780 nm, with a repetition frequency of approximately 100 MHz, a pulse duration of 150 fs, and a maximum power of 50 mW. The laser beam was scanned in the sample plane with a high-resolution galvo-based system. A liquid photoresist immersed the lens in an IP-Dip photoresist during immersion laser lithography (DILL - Dip in Laser Lithography). A laser power of 20 mW and a scanning speed of 10,000 m/s were used. By using 2PP, IP-Dip photoresist polymerized in the exposed volume [34]. After polymerization, the sample was developed in propylene glycol monomethyl ether acetate (PGMEA). The structure was fabricated on a glass substrate, which is shown in Fig. 3.4c. Once the optical fiber was inserted into the prepared mechanical part, the structure was peeled off from the glass substrate. The scanning electron microscope (SEM) image revealed a smooth surface, indicating high optical quality [31].

3.2.5 Measurement

The fabricated MMI structure was attached to the end of the SMF. Critical factors that impose losses and influence the shape of the output interferential maxima are the SMF and MMI splitter alignment and the consistent connection, ideally without an air gap. The centered SMF is attached to the micromechanical offset and clamped to the structure. The process of attaching the SMF to the structure is monitored by a microscope with a camera and for higher precision, visible light is coupled to the fiber to monitor the transmitted signal. After the optical fiber was attached to the structure, the structure was removed from the glass substrate.

The optical properties of the developed 3D 1 × 4 MMI splitter were experimentally analyzed and measured using a highly resolved near-field scanning optical microscope (NSOM) with a lateral resolution of around 100 nm. The waveguide input was directly connected to a laser source that emits at 1550 nm and is coupled with an SMF. A femtowatt InGaAs detector (900 - 1700 nm) was utilized to measure the near-field distribution close to the output waveguides [31].

The measured optical field intensity distribution for each S-Bend output

waveguide is shown in Fig. 3.5. As can be seen, the measured intensity distribution confirms 1 × 4 splitting. Also, a weak presence of a higher-order mode at the first two output waveguides was observed in the near-field image in Fig. 3.5a and Fig.3.5b [31].

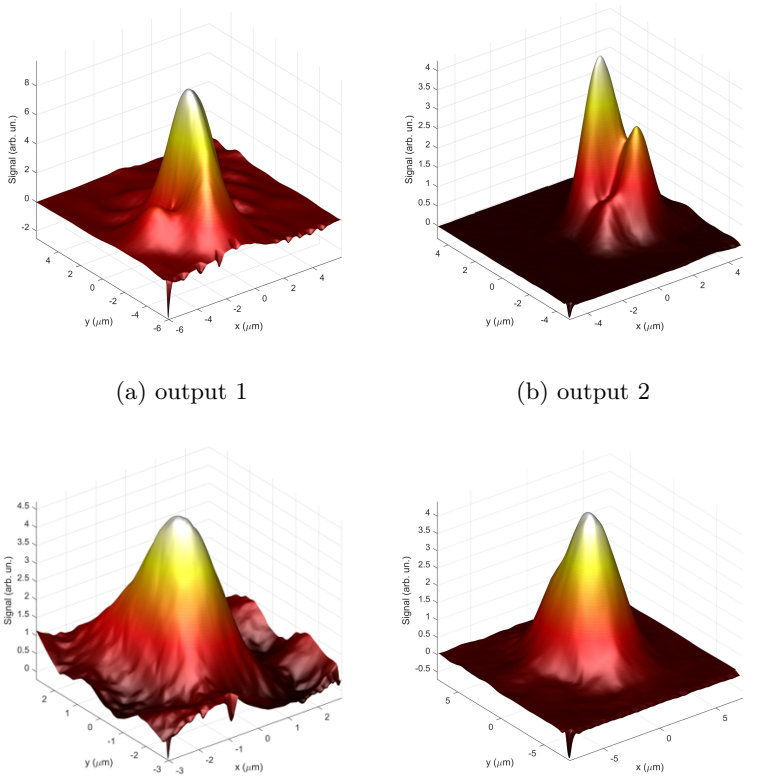

(a) output 1

(b) output 2

(c) output 3

(d) output 4

Figure 3.5: Near-field images of measured intensity distribution at the end of each output waveguide [31].

3.3 3D 1×6 multimode interference splitter

A novel 3D rectangular structure of 1 × 6 MMI coupler with direct integration to the end facet of standard single-mode optical fiber is presented using a robust mechanical structure. The motivation for this design was an asymmetric

2×3 distribution of outputs, as it was not published yet.

Figure 3.6a shows the schematic of a polymer-based 3D 1×6 MMI splitter consisting of an SMF input, input waveguide in the form of linear taper, an MMI coupler (splitting part), and six output linear tapers. The input linear taper was used to couple the optical signal from the SMF to the MMI coupler. At the SMF side, the input cross-section of the taper was set to (10×10) µm^2, and at the input to the MMI coupler, it was set to (4×4) µm^2. The length of the linear taper was optimized to $L_T(in) = 40$ µm. The size of the MMI coupler needs to be determined to reach the optimum output power with minimum losses. In the case of six outputs, the 3D MMI coupler has a rectangular arrangement of output signals, i.e., the matrix of m rows and n columns. Therefore, the width W_{MMI} and height H_{MMI} of the MMI coupler had to be determined. The width of the MMI coupler was set to $W_{MMI} = 24$ µm and the height $H_{MMI} = 20$ µm. For such a cross-section, the length L_{MMI} was determined to be 193 µm. Finally, six linear output tapers were connected to the end of the MMI coupler. Correct signal distribution is essential to achieve high uniformity of split optical signal. Therefore, the linear output tapers were placed considering the width and height of the MMI coupler and were spaced equally apart. The cross-section at the taper origin was set to (5.5×5.5) µm^2 and at the exit, it was (4×4) µm^2. The taper length was optimized for maximum intensity at $L_T(out) = 25$ µm [35]. A supporting stable mechanical structure shown in Fig. 3.6c was again additionally developed to improve the mechanical stability of the coupler.

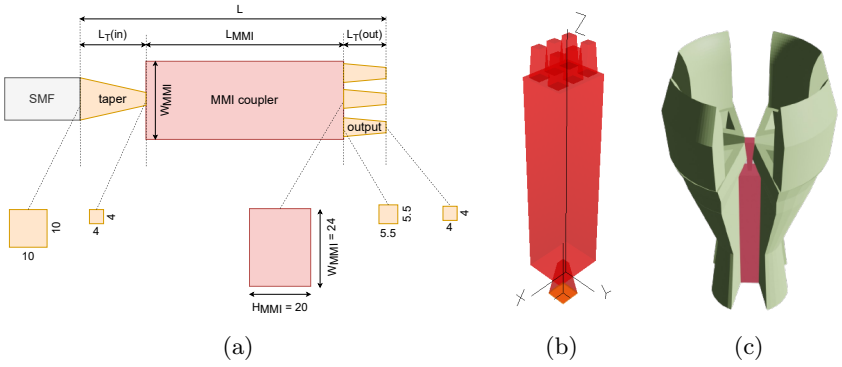

(a) (b) (c)

Figure 3.6: (a) Schematic view of 3D 1×6 MMI splitter (side view), (b) 3D design of 1×6 MMI coupler in RSoft tool, (c) 3D 1×6 MMI splitter with a mechanical construction [35].

3.3.1 Simulation

The simulation results of intensity distribution at the end of the multimode coupler are shown in Fig. 3.7a for TE polarization and in Fig. 3.7b for TM polarization. The insertion loss of the simulated 1 × 6 MMI coupler was IL = -7.97 dB, with non-uniformity of the output signal distribution of ILu = 0.02 dB for TE polarization and IL = 7.81 dB with non-uniformity of ILu = 0.01 dB for TM polarization [35].

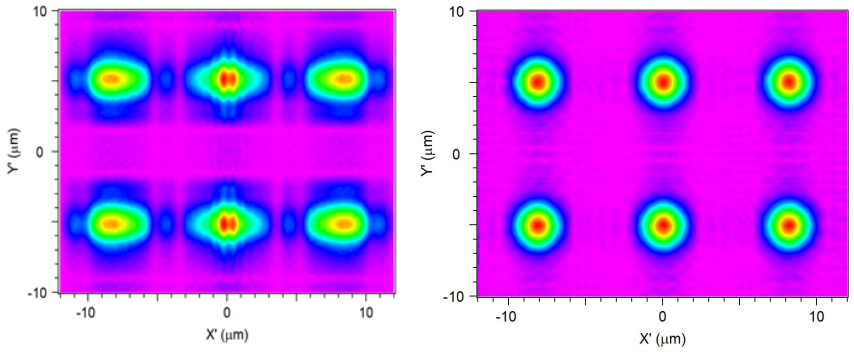

(a) (b)

Figure 3.7: Simulation of intensity distribution at the end of 3D 1 × 6 MMI coupler: a) TE polarization, b) TM polarization [35].

3.3.2 Fabrication and measurement

The fabrication process was again done by the project partner at the Department of Optics and Photonics at the University of Žilina. In experiments, the designed MMI splitter was fabricated without output tapers to be able to verify the correct splitting of the input signal. The fabrication process and measuring of intensity distribution were the same as in the case of 3D 1 × 4 MMI splitter as described in Subsection 3.2.4 and 3.2.5. The optical properties of the prepared structure were experimentally determined using NSOM analysis, which was also used to analyze the 3D 1 × 4 MMI splitter. The analysis provides a high-resolution view of the field distribution at the end of the MMI coupler, shown in Fig. 3.8. Again, the same optical fiber tip with a thin aluminum layer and a resolution better than 100 nm was used as the fiber probe. As shown in Fig. 3.8, the measured intensity distribution confirms 1 × 6 splitting. The simulation and near-field image observed a weak presence of the higher-order mode at the end of the MMI

coupler. Suppressing the higher-order mode requires further optimization of the structure [35].

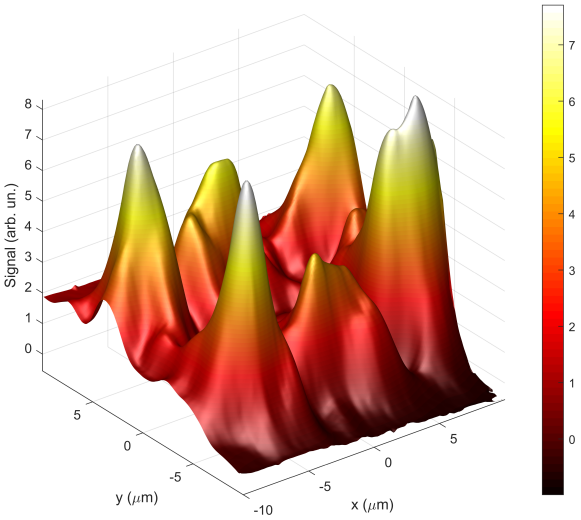

Figure 3.8: Near-field image of the measured intensity distribution at the end of 3D 1 × 6 MMI coupler [35].

4. Silicon Nitride-based components for medical applications

This chapter presents the design, simulation and optimization of 1 × 8 Y-branch splitter and 1 × 8 MMI splitter. The design of the 1 × 8 MMI splitter was further optimized based on technological limitations and it was fabricated in the International Laser Centre (ILC CVTI SR) in Bratislava [36]. The design, simulation and optimization of the splitters were performed by a commercial photonics simulation engine tool - BeamPROP by RSoft Photonic Suite, which uses the beam propagation method.

4.1 Material platform

The optical waveguide structure used for designing the optical splitter is a buried rectangular channel waveguide. The optical splitter was designed and simulated at the operating wavelength, $\lambda = 850$ nm. For this operating wavelength the core of the waveguide structure is Si_3N_4 having $n_c = 1.925$, which is transversely surrounded by the SiO_2 cladding layer of refractive index $n_{cl} = 1.4575$. The width of the waveguide core is 0.8 µm, and the height is 0.16 µm [37].

4.2 1×8 Y-branch splitter

A 1 × 8 Y-branch splitter structure comprises an input waveguide, splitting waveguides, and output waveguides, as presented in Fig. 4.1. The lengths of input and output waveguides were tested and set to $L(in) = L(out) = 10$ µm. The waveguides placed between the input/output waveguides are used to evenly split the optical signal into S-Bend segments in the cascade system leading to the output waveguides. The splitting waveguides had an Arc S-Bend shape. In order to keep the overall length of the splitter as short as possible, each Y-branch was individually scanned in the selected length range, and an optimized length was selected for the final design structure, where $L_1 = 460$ µm, $L_2 = 200$ µm and $L_3 = 160$ µm. The spacings between the individual Y-branches were also tested and determined as follows: $P_1 = 16$ µm, $P_2 = 8$ µm, and $P_3 = 4$ µm [38]. The simulation of the 1 × 8 Y-branch splitter in the BeamPROP tool is shown in Fig. 4.2. The insertion loss reached IL = -9.37 dB and non-uniformity $ILu = 0.68$ dB for TE polarization. The insertion loss for a TM polarization was almost the same, namely IL = -9.95 dB and slightly higher non-uniformity $ILu = 0.98$ dB.

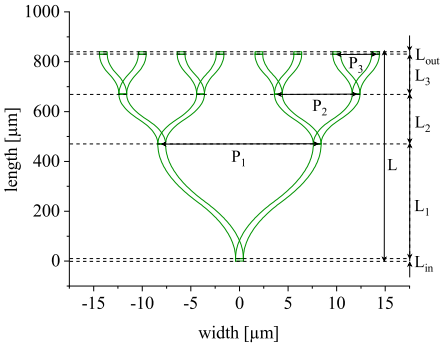

Figure 4.1: Schematic view of the proposed 1 × 8 Y-branch splitter [38].

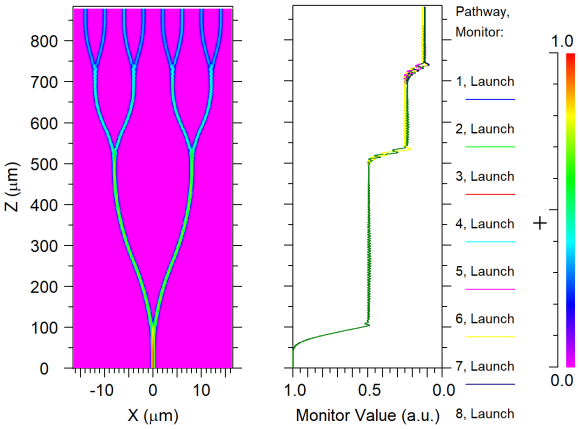

Figure 4.2: (a) Simulation of 1 × 8 Y-branch splitter in XZ direction, (b) simulated optical power distribution from input to output waveguides [38].

4.3 1×8 multimode interference splitter

Figure 4.3 shows the geometry of the 1 × 8 MMI splitter with eight S-Bend output waveguides. The length of input waveguide $L(in)$ was 10 µm, MMI coupler width W_{MMI} was 25 µm and MMI coupler length L_{MMI} was 174 µm. The length L_T and the input width of the linear output tapers were tested to collect the maximum intensity from the MMI coupler into output waveguides. The input width was set to 1.4 µm, and the output width was equal to

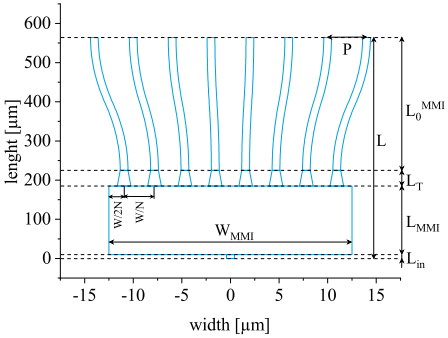

Figure 4.3: Schematic view of the proposed 1 × 8 MMI splitter with eight S-Bend output waveguides [38].

the width of the waveguide (0.8 µm). The length of the linear output tapers was set to 40 µm. The spacing between the linear output tapers was 3.125 µm. The length of the output branching waveguides L_0^{MMI} was 340 µm for TE and TM polarization. The port pitch P between the output waveguides was set to 4 µm [38].

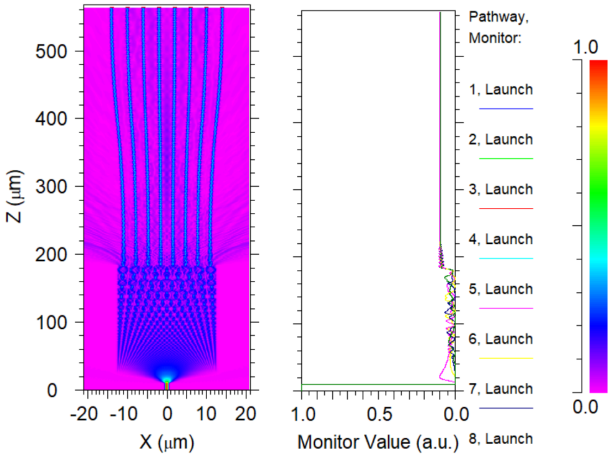

(a) (b)

Figure 4.4: (a) Simulation of 1 × 8 MMI splitter in XZ direction, (b) simulated optical power distribution from input to output waveguides [38].

The simulation of the MMI splitter with S-Bend output waveguides is shown in Fig. 4.4. The structure was designed with pathway monitors. Pathway monitors show the field propagation through the structure and how much of the field is converted into the output waveguides. Based on that, the optical performance is calculated and evaluated. The insertion loss for TE polarization was IL = -10.22 dB, and non-uniformity was ILu = 0.18 dB. The insertion loss for TM polarization was IL = -10.14 dB and a non-uniformity ILu = 0.09 dB.

4.4 Optimization of 1×8 multimode interference splitter for fabrication

Due to the limitations of the fabrication process in ILC CVTI SR in Bratislava, the final MMI structure had to be further optimized. The main reason was that the linear output tapers were placed too close to each other, which caused problems during the etching process. The other reason is that a 9 µm optical fiber will be fed to the MMI structure for the characterization. Therefore, the input waveguide position should be at least 5-10 µm from the last output waveguide, ideally more.

The optimized design is shown in Fig. 4.5. First, the MMI coupler width W_{MMI} was increased from 25 µm to 30 µm, and the MMI coupler length was extended from L_{MMI} = 185 µm to L_{MMI} = 254 µm, see in Fig. 4.5a. The size and length of the linear output tapers remained unchanged. The length of the S-Bend output waveguides has also not changed. However, the spacing between the linear output tapers increased, so the spacing from one output to the other was 3.75 µm, which was sufficient for the etching process.

In addition to the linear input waveguide $L(in)$, an S-Bend input waveguide and inverse taper were added in front of the MMI coupler. Two inputs with different offsets were designed. They consist of the same linear input waveguide and inverse taper L_{inv}. The length of the linear input waveguide was $L(in)$ = 40 µm. The length of the inverse taper was L_{inv} = 40 µm. The width of the inverse taper at the beginning was 0.8 µm, and at the end, 2 µm. The S-Bend input waveguide, shown in Fig. 4.5b, had an offset of W_B = 33 µm and a length L_B = 900 µm. Then the starting point of the input waveguide, where the optical fiber will be connected, is distanced by O = 12 µm from the last output waveguide. The MMI structure in Fig. 4.5c had an S-Bend input waveguide offset set to W_B = 73 µm and a length of L_B = 2100 µm. The starting point of the input waveguide is, in this case, distanced by O = 52 µm from the last output waveguide.

The S-Bend input waveguide lengths and offsets were chosen, considering

insertion losses and non-uniformity at output waveguides. The results of both structures for both polarizations are shown in Tab. 4.1. In both cases, lower insertion loss values were achieved compared to the 1 × 8 MMI splitter design with an MMI coupler width of 25 µm. The insertion losses of MMI splitters were similar in both cases of S-Bend input waveguide offsets. The insertion loss of the 1 × 8 MMI splitter with the S-Bend input waveguide offset of 33 µm was IL = -9.72 dB and a non-uniformity ILu = 0.24 dB for TE polarization. For TM polarization, insertion loss was ILu = -9.54 dB and non-uniformity ILu = 0.13 dB. The footprint of the structure reached (1624 × 54) µm^2. The insertion loss of 1 × 8 MMI splitter with the S-Bend input waveguide offset of 73 µm was the same for both polarizations, IL = -9.84 dB. Only non-uniformity differs for TE polarization, ILu = 0.07 dB and TM polarization, ILu = 0.23 dB. The footprint of the structure reached (2824 × 94) µm^2. These two configurations of 1 × 8 MMI splitter were sent for a photolithography mask fabrication.

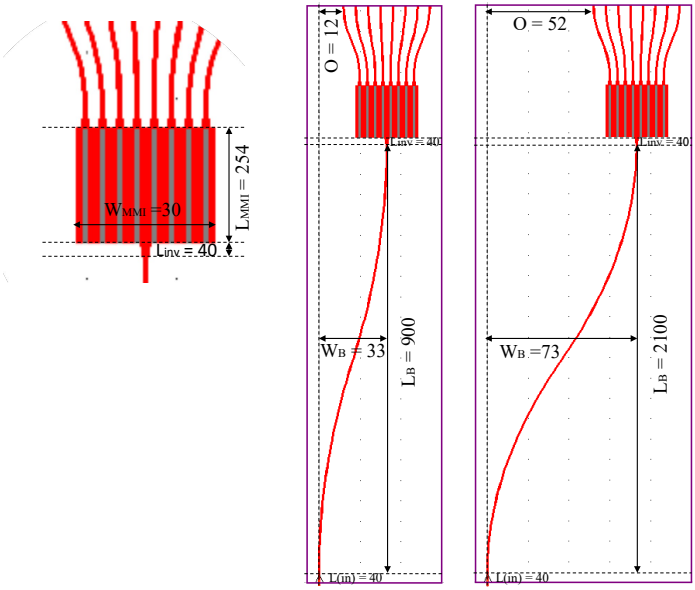

Figure 4.5: Optimized design of 1 × 8 MMI splitter: (a) detailed view of MMI structure, (b) S-Bend input waveguide with an offset of 33 µm, (c) S-Bend input waveguide with an offset of 73 µm.

Table 4.1: Summary results of the 1 × 8 MMI splitter with different S-Bend input waveguide offsets and lengths for both polarizations.

MMI splitter with S-Bend input offset, W_B [µm]	Polarization	Non-uniformity, ILu [dB]	Insertion loss, IL [dB]	Footprint [µm^2]
33	TE	0.24	-9.72	1624 × 54
	TM	0.13	-9.54	
73	TE	0.07	-9.84	2824 × 94
	TM	0.23	-9.84	

4.5 Fabrication

The photolithography mask for fabrication was designed in the Klayout tool [39] by a project partner at the Institute of Electronics and Photonics from Slovak University of Technology in Bratislava [40]. The fabrication process was done by a project partner in ILC CVTI SR in Bratislava. Since the fabrication is not the main focus of the thesis, this section provides only brief information about the process. The fabrication process of 1 × 8 MMI splitters based on silicon nitride material consists of deposition of Si_3N_4 core layer, photolithography, dry etching of the Si_3N_4 layer and deposition of SiO_2 cladding layer. The Plasma Enhanced Chemical Vapor Deposition (PECVD) [41] process was used to deposit the core layer using an Oxford Instruments Plasmalab80Plus. The photolithography was done by mask aligner and exposition chamber (MA/BA6, SUSS MicroTec SE). The dry etching process of the Si_3N_4 layer took place in the inductively coupled plasma reactive ion etching (ICP/RIE) Plasmalab System 100 chamber from Oxford Instruments. The same PECVD process performed the deposition of the SiO_2 cladding layer [41] as the deposition of the Si_3N_4 core layer of the waveguide.

4.6 Characterisation

The etched width of the fabricated structure was verified using the optical microscope ZEISS Axioscope 5 [42] at the Institute of Electronics and Photonics in Bratislava [40].

In Fig. 4.6a, the width of the S-Bend input waveguide was measured. The width of the S-Bend input waveguide was 2.561 µm, which differs by ≈ 1.8 µm from the designed width of 0.8 µm. Figure 4.6b shows the mea-

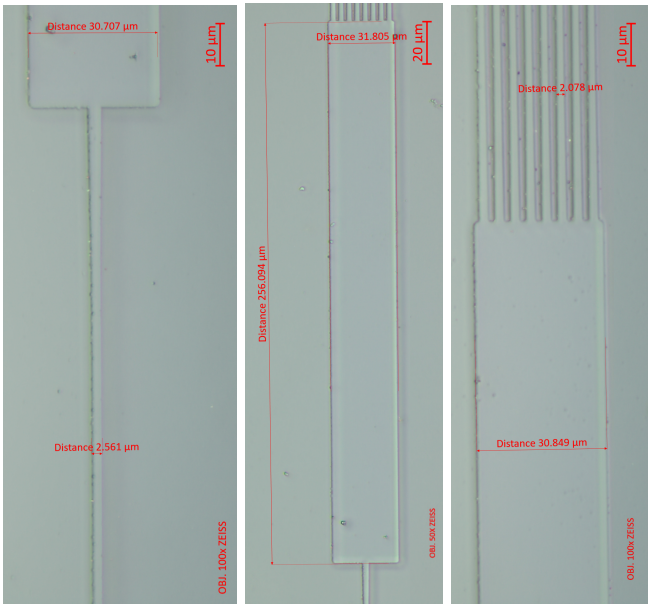

(a) (b) (c)

Figure 4.6: Images of fabricated 1 × 8 MMI splitter from high accuracy microscope ZEISS Axioscope 5: (a) measured S-Bend input waveguide width and MMI coupler width, (b) measured MMI coupler width and length, (c) measured MMI coupler width and linear output taper width.

sured MMI coupler length of 256.094 µm, which differs by 2.094 µm from the originally designed 254 µm length. The width of the MMI coupler was measured in three different parts (beginning (30.707 µm), end (31.805 µm) and middle (30.849 µm)) and the measurements are shown in Figs. 4.6a, 4.6b and 4.6c. The measured MMI coupler width differs maximum by 1.805 µm from the designed width of $W_{MMI} = 30$ µm. The measurement of the linear output taper width of 2.078 µm (designed from 1.4 µm to 0.8 µm) is shown in Fig. 4.6c. As can be seen, the width characterization of the fabricated 1 × 8 MMI splitters differs approximately in the range of ≈ 0.707 to ≈ 1.808 µm from the original design values.

For more accurate analysis, atomic force microscopy (AFM) was used to verify the etched depth of the structure and the widths of the individual parts of the fabricated 1 × 8 MMI splitter. The left side of Fig. 4.7 shows the topography map of a part of the MMI coupler with eight output linear tapers. The green line measured the width and etched depth of the MMI coupler.

The red cursors on the green line measured the width of the MMI coupler at 30.175 µm, which corresponds with the designed width $W_{MMI} = 30$ µm (in Section 4.4). The green cursors on the green line measured the MMI coupler etched depth of 0.21 µm, which differs from the originally designed value of 0.16 µm by 0.05 µm. The green line profile of the measured MMI coupler cross-section is shown on the right-up side in Fig. 4.7.

The red line measured the width and etched depth of the output linear tapers. The red cursors on the red line measured the 1.65 µm width of the output tapers and the green cursor measured the etched depth of the output tapers of 0.213 µm. The red line profile of the measured output tapers cross-section is shown on the right-bottom side in Fig. 4.7.

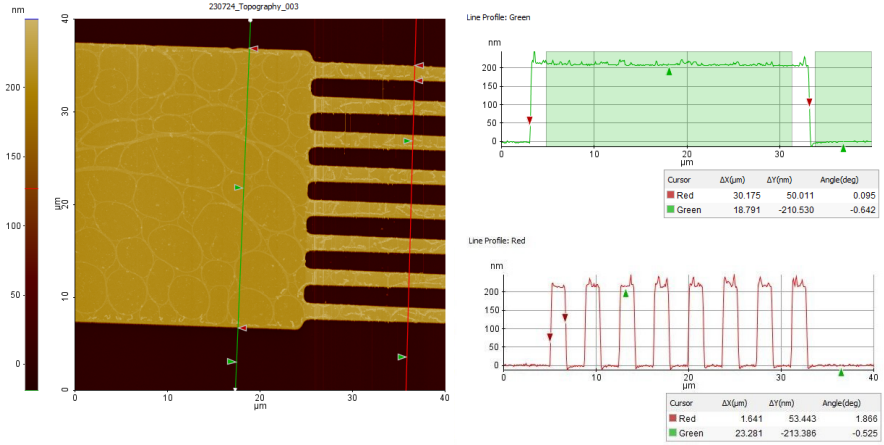

Figure 4.7: Topography map of the fabricated 1 × 8 MMI splitter.

The results of the widths of the splitter structure by AFM were more accurate compared to the measured widths using an optical microscope. However, the results from AFM also show an inaccuracy in the fabrication process, namely, excessively deep etching of the waveguide structure, which could be adjustable by shortening the etching time and optimization of the photolithography process.

Conclusion

The aim of this dissertation thesis was the design, simulation and optimization of passive optical components. The thesis is primarily concerned with designs based on two fundamental principles of optical signal splitting: the Y-branch splitter and the multimode interference splitter approach. These splitters have been principally designed for telecommunication and medical applications using three established material platforms. Two different software tools were used for design and simulation using the beam propagation method.

The first practical objective was to design the splitters based on the SoS material platform for a telecommunications wavelength of 1550 nm. The Y-branch splitters were designed, simulated and optimized up to 1:128 splitting ratio. Detailed analysis of the impact of the S-Bend output waveguide shapes was presented, focusing on the length optimization of the whole splitter structure. For a standard waveguide core cross-section of (6 × 6) µm^2, the shortest length was achieved for 1 × 128 Y-branch splitter with Sine S-Bend waveguide shape. In the next optimization step, the waveguide core cross-section was reduced to (5.5 × 5.5) µm^2 and to further (5 × 5) µm^2 to suppress higher-order modes and support only fundamental mode propagation. The results showed that the smaller waveguide cross-section ensures not only a strong improvement of the optical performance but also a smaller footprint of the splitter. The splitter with Sine S-Bend waveguide shape was again leading in the case of waveguide cross-section of (5 × 5) µm^2. The splitter with an Arc S-Bend waveguide shape achieved better optical properties, but the splitter length was longer than the splitter with a Sine S-Bend waveguide shape. Considering both, the footprint and the performance optimization, the splitter with Sine S-Bend waveguide shape and waveguide cross-section size of (5.5 × 5.5) µm^2 had reached superior results. Compared to the originally proposed 1 × 128 Y-branch splitter with waveguide core cross-section of (6 × 6) µm^2 and Arc S-Bend waveguide shape, which reached a footprint of (163800 × 16129) µm^2, the 1 × 128 Y-branch splitter with waveguide core cross-section of (5.5 × 5.5) µm^2 and Sine S-Bend waveguide shape has shrank to the footprint of (75700 × 16129) µm^2, which is less than half of the original length. The insertion losses reduced from -22.51 dB to -21.86 dB and the non-uniformity from 2.05 dB to 1.30 dB.

For the first time, an MMI splitter with a splitting ratio of 1:128 was introduced and compared with a conventional 1 × 128 Y-branch splitter with waveguide cross-section of (6 × 6) µm^2. The length-optimized 1 × 128 Y-branch splitter results show low insertion losses and high uniformity of the split optical signal at output waveguides. In the case of 1 × 128 MMI

splitter, applying linear output tapers together with the length optimization of the output waveguides led to even smaller non-uniformity and lower insertion losses. The results confirmed the advantages of the MMI splitter over the Y-branch splitter. The 1 × 128 MMI splitter reached better optical properties regarding non-uniformity and insertion loss. At the same time, the advantage of the small footprint of the MMI splitter was confirmed. Mainly, the non-uniformity difference between the Y-branch splitter and MMI splitter was more than half and the final length of the MMI splitter reached less than half the size of the Y-branch splitter as well. It has also been confirmed that the MMI splitter based on a silica-on-silicon waveguide is less polarization-dependent.

Subsequently, in the second practical objective, the thesis introduced a new design of a multimode interference splitter based on an IP-Dip polymer material platform in a three-dimensional configuration. A novel 3D 1 × 4 MMI splitter with S-Bend output waveguides has been developed. The splitter was designed for an operating wavelength of 1550 nm. The waveguide core cross-section was optimized from (2 × 2) µm^2 to (4 × 4) µm^2 and the input waveguide of the splitter was adapted for connection to optical single-mode fiber. The 3D MMI coupler was then designed in a square array with four S-Bend output waveguides. The optimal size of the multimode interference splitter and the optimal length of the outputs were determined based on minimum insertion losses and minimum non-uniformity. The whole structure was fabricated together with the supporting mechanical structure in two single steps using direct laser writing technology. The splitting of the optical signal was verified by near-field measurement.

The variability of the MMI splitter design in the 3D configuration was also verified by changing the MMI coupler design from a square array to a rectangular array to split the signal into six outputs. The 1 × 6 MMI splitter without linear output waveguides was also fabricated with the supporting mechanical structure in a single step using direct laser writing technology. The measured and simulated results at the end of the 1 × 6 MMI coupler confirmed the 1 × 6 splitting with the presence of the first weak higher-order mode.

The final part of the thesis was devoted to the design of the 1 × 8 Y-splitter and the 1 × 8 MMI splitter based on the silicon nitride material platform. Both optical components were designed for a wavelength of 850 nm and their waveguide core cross-section was (0.8 × 0.16) µm^2. The 1 × 8 MMI splitter was further optimized for the fabrication process using the PECVD and the fabricated structure was characterized by topological and optical methods. In this case, it was shown how the material platform significantly affects the dimensions of the photonic structures. Compared to the standard SoS waveg-

uide structures, their length was several times smaller and reached similar optical properties. These structures are thus a suitable candidate for miniaturization and integration on a chip in the new, progressively developing field of biophotonic or medical applications.

Main contributions of the dissertation thesis

Based on the objectives and achieved results during the writing of the dissertation thesis, the following main contributions are presented:

Objective 1

- New knowledge has been gained in the field of passive optical components and their use in two industrial fields, namely in telecommunication and medical applications. During the dissertation study, the skills were gained in using two commercial photonics software tools with implemented beam propagation method, which is relevant for the design, simulation and optimization of specific photonics waveguide structures such as Y-branch and MMI splitters.

Objective 2

- Y-branch splitters based on the SoS material platform were designed and simulated up to a splitting ratio of 1:128 for the telecommunication operating wavelength of 1550 nm. The optical properties of the structures were analyzed. According to minimum insertion losses, non-uniformity and background crosstalk, the structures were further optimized based on the splitter length, waveguide core size, and S-Bend output waveguide shapes.
- Design, simulation and optimization of a novel 1 $\times$ 128 MMI splitter was presented and the results were compared with the 1 $\times$ 128 Y-branch splitter.
- Supporting program was developed to automatically calculate the optical performance parameters for splitters with a higher splitting ratio.

Objective 3

- A 3D structure of 1 $\times$ 4 MMI splitter with S-Bend output waveguides based on IP-Dip polymer was designed and simulated for a wavelength of 1550 nm. The parameters of the splitter were optimized in multiple steps according to the minimum insertion losses, non-uniformity and fabrication limitations.

The 3D 1 × 4 MMI splitter was fabricated using 3D laser lithography directly attached to the SMF. The near-field analysis of the optical properties verified that the measured interference field at the output of the MMI splitters corresponds to the splitting ability shown in the simulation.

- The capabilities of the multimode interference effect have been verified in the design and simulation of an asymmetric rectangular polymer-based 3D 1 × 6 MMI coupler, which was also fabricated using 3D laser lithography. Near-field measurements also confirmed the splitting ability of the MMI coupler.

Objective 4

- Design, simulation and optimization of Si_3N_4-based 1 × 8 Y-branch and 1 × 8 MMI splitters for the medical operating wavelength of 850 nm were presented. The optimized 1 × 8 MMI splitter was fabricated by PECVD and the fabricated splitter was characterized by topological and optical methods.

Resumé

Pasívny optický delič je planárna vlnovodná štruktúra, ktorá rozdelí optický zväzok, naviazaný z optického vlákna do vstupného vlnovodu, na dva alebo viac optických zväzkov. Rovnako môže optický delič zlúčiť viac optických zväzkov do jedného spoločného zväzku pri použití optického deliča v opačnom smere.

Na delenie vstupného optického signálu na N výstupných signálov sa používajú dve základné metódy. Najznámejším spôsobom je použitie série vlnovodov v tvare Y zapojených do kaskády (nazývaných aj Y-delič). Pri tomto spôsobe delenia signálu je v ideálnom prípade jednoduchého Y-deliča polovica výkonu vstupného optického zväzku naviazaná do jednej vetvy Y-deliča a druhá polovica do druhej vetvy Y-deliča. Bod, v ktorom sa vlnovod začína rozdeľovať na dva je však technologicky veľmi náročné realizovať, čo vo všeobecnosti vedie k nerovnomernému rozdeleniu optického výkonu do výstupných vlnovodov. Na druhej strane majú tieto deliče dve významné výhody, a to nezávislosť od polarizácie a vlnovej dĺžky, t. j. jeden Y-delič je možné použiť na rozdelenie optických signálov v celom telekomunikačnom vlnovom rozsahu.

Na rozdiel od Y-deliča sú multimódové interferenčné deliče (MMI z angl. mulimode interference) založené na delení optického signálu na báze samozobrazovacieho efektu v multimódovej časti deliča. V tejto časti dochádza k superpozícii vybudených módov s rôznymi rýchlosťami šírenia, ktoré reprodukujú profil vstupného optického poľa do jedného alebo viacerých maxím v pravidelných intervaloch pozdĺž smeru šírenia signálu. Ukončením MMI časti v určitej dĺžke možno získať N výstupných signálov. MMI deliče umožňujú rozdeliť signál do veľkého počtu výstupných signálov so stabilným deliacim pomerom, čo zabezpečuje rovnomerné rozdelenie optického výkonu do všetkých výstupných vlnovodov. Okrem toho sú MMI deliče potenciálne kratšie v porovnaní s Y-deličmi. Ďalšou výhodou je ich dobrá výrobná tolerancia, pretože delenie prebieha v multimódovej časti deliča. Ich hlavná nevýhoda vyplýva zo skutočnosti, že dĺžka multimódovej časti deliča závisí od vlnovej dĺžky, t. j. MMI deliče sú navrhnuté výlučne pre jednu vlnovú dĺžku a môžu pracovať len v úzkom pásme vlnových dĺžok. Sú tiež závislé od polarizácie; ukázalo sa však, že v prípade silne viazaných vlnovodných štruktúr je táto závislosť minimálna.

Výkonové charakteristiky optických deličov závisia najmä od optických vlastností materiálov použitých na výrobu vlnovodov, ale aj od tvaru použitej vlnovodnej štruktúry. Jadro tejto štruktúry tvorí aktívna časť s vyšším

indexom lomu ako má materiál, ktorý túto aktívnu časť obklopuje. V tejto dizertačnej práci sú použité tri rôzne materiálové platformy s kanálkovým tvarom vlnovodu, na základe ktorých sú navrhnuté Y-deliče a MMI deliče.

Na návrh, simuláciu a optimalizáciu pasívnych optických prvkov v tejto dizertačnej práci sú použité komerčné fotonické softvérové nástroje, a to softvér OptiBPM od spoločnosti Optiwave a softvér BeamPROP od spoločnosti RSoft Photonics CAD Suite. Tieto fotonické softvérové nástroje používajú metódu šírenia optického zväzku (BPM z angl. beam propagation method) na výpočet šírenia optického žiarenia v navrhovaných pasívnych optických prvkoch.

Prvky na báze oxidu kremíka pre telekomunikačné aplikácie

Prvá materiálová platforma, použitá na návrh optických vlnovodov v tejto práci, je platforma na báze oxidu kremíka na kremíku. Index lomu jadra v takomto vlnovode je $n_c = 1.456$ a index lomu okolitého materiálu (z angl. cladding) je $n_{cl} = 1.455$. Rozmery jadra vlnovodu sú (6×6) µm^2.

Optické deliče boli navrhované pre telekomunikačnú vlnovú dĺžku 1550 nm. Y-deliče boli navrhnuté, simulované a optimalizované až do deliaceho pomeru 1:128. Optimalizácia rozmerov Y-deličov predstavuje dôležitý krok po návrhu, ktorej cieľom je dosiahnúť minimálne rozmery deličov bez zhoršenia ich optických vlastností. Optimalizácia pozostávala z niekoľkých krokov:

- optimalizovala sa dĺžka jednotlivých častí Y-deliča pozostávajúcich z vlnovodov zakrivených v tvare S (S-Bend),
- veľkosť jadra vlnovodu bola zmenšená a dĺžka Y-vlnovodov bola optimalizovaná pre novú veľkosť jadra vlnovodu,
- na potlačenie rozptylu optického žiarenia vo vlnovodoch sa použili a skúmali všetky tvary S-zakrivených vlnovodov (arcus, sínus, kosínus),
- vybrané tvary S-zakrivených vlnovodov boli použité na návrh Y-deličov s optimalizovanou veľkosťou jadra vlnovodu,
- bol vyvinutý podporný skript na automatizované vyhodnotenie optických vlastností navrhnutých deličov s vysokými pomermi delenia.

Pre štandardnú veľkosť jadra vlnovodu o priereze (6×6) µm^2 bola dosiahnutá najkratšia dĺžka navrhnutého 1×128 Y-deliča použitím vlnovodov v sínusovom tvare. V ďalšom kroku optimalizácie bol prierez jadra vlnovodu zmenšený na (5.5×5.5) µm^2 a následne na (5×5) µm^2, za účelom eliminácie vyšších módov a na podporu šírenia iba základného módu vo vlnovode. Výsledky ukázali, že menší prierez jadra vlnovodu zaručí zlepšenie optických

vlastností deliča a zároveň umožní zmenšenie štruktúry deliča. Y-delič so sínusovými vlnovodmi o priereze vlnovodu s rozmermi (5 × 5) µm^2 dosiahol najlepšie výsledky. Y-delič s arcus tvarom vlnovodov dosiahol lepšie optické vlastnosti, ale dĺžka deliča bola väčšia ako dĺžka deliča so sínusovým tvarom vlnovodov. Pri zohľadnení optimalizácie veľkosti deliča a aj výkonu, dosiahol najlepšie výskedky delič so sínusovým tvarom vlnovodu a prierezom jadra vlnovodu o veľkosti (5.5 × 5.5) µm^2. V porovnaní s pôvodne navrhnutým Y-deličom 1 × 128 o priereze jadra vlnovodu (6 × 6) µm^2 a arcus tvarom vlnovodu, ktorý dosiahol veľkosť deliča (163800 × 16129) µm^2, Y-delič 1 × 128 s prierezom jadra vlnovodu (5.5 × 5.5) µm^2 a sínusovým tvarom vlnovodu bol zmenšený na veľkosť (75700 × 16129) µm^2, čo predstavuje viac ako polovičné skrátenie pôvodnej dĺžky deliča. Vložné straty sa zmenšili z -22.51 dB na -21.86 dB a nerovnomernosť rozdelenia signálu klesla z 2.05 dB na 1.30 dB.

Po prvýkrát bol navrhnutý MMI delič s deliacim pomerom 1:128 a bol porovnaný so štandardným Y-deličom 1 × 128 o priereze vlnovodu (6 × 6) µm^2. Výsledky optimalizovaného 1 × 128 Y-deliča potvrdzujú nízke vložné straty a vysokú rovnomernosť rozdelenia optického signálu do výstupných vlnovodov. V prípade MMI deliča 1 × 128 sa použitím špeciálnych vlnovodných štruktúr spolu s optimalizovanou dĺžkou výstupných vlnovodov dosiahlo rovnomernejšie rozdelenie optického signálu ešte s nižšími vložnými stratami. Výsledky potvrdili výhody MMI deliča v porovnaní s Y-deličom. Konečná veľkosť MMI deliča 1 × 128 bola (74422 × 16129) µm^2, čo je menej ako polovica dĺžky Y-deliča, (163800 × 16129) µm^2. Potvrdilo sa tiež, že MMI delič na báze oxidu kremíka na kremíku je menej závislý od polarizácie.

Prvky na báze polymérov pre telekomunikačné aplikácie

Následne v rámci druhej praktickej dizertačnej tézy bol navrhnutý MMI delič 1 × 4 s výstupnými vlnovodmi na báze IP-Dip polymérneho materiálu v trojrozmernej konfigurácii (3D z angl. three dimensional). Index lomu jadra vlnovodu je $n_c = 1.53$ a index lomu obalu je $n_{cl} = 1.3997$. Prierez jadra vlnovodu bol optimalizovaný z (2 × 2) µm^2 na (4 × 4) µm^2 a vstupný vlnovod deliča bol prispôsobený na pripojenie k monomódovému optickému vláknu. Delič bol navrhnutý pre vlnovú dĺžku 1550 nm.

Najprv bol navrhnutý planárny (2D z angl. two dimensional) MMI delič 1 × 4, ktorý tvoril základ pre návrh MMI deliča 1 × 4 v 3D usporiadaní. Tento delič bol vyrobený pomocou 3D litografie. Štruktúra 3D MMI deliča 1 × 4 bola optimalizovaná pre nasledujúce parametre:

- dĺžka výstupných vlnovodov bola optimalizovaná a skúmali sa ich

optické vlastnosti,

- veľkosť jadra vlnovodu bola optimalizovaná za účelom zlepšenia optických vlastností deliča,
- potrebná bola zmena materiálu obalovej vrstvy z polyméru na vzduch s indexom lomu $n_{cl} = 1$, pretože bolo veľmi náročné použiť materiál PDMS ako obalovú vrstvu pri výrobnom procese,
- bola navrhnutá špeciálna vlnovodná štruktúra na vstupe MMI deliča na pripojenie optického vlákna a súčasne sa optimalizoval prierez MMI časti deliča,
- bola navrhnutá špeciálna vlnovodná štruktúra na výstupe MMI deliča, na ktorú boli napojené výstupné vlnovody, ktoré boli tiež optimalizované.

Vložné straty (IL z angl. insertion loss) optimalizovaného 3D MMI deliča 1×4 boli IL = -10.027 dB s nerovnomernosťou rozloženia výstupného signálu (ILu z angl. insertion loss uniformity) $ILu = 0.098$ dB. Aj napriek tomu, že vložné straty IL sa zvýšili približne o 2.3 dB a nerovnomernosť rozloženia výstupných signálov ILu sa tiež zvýšila o 0.09 dB, v porovnaní s predchádzajúcou štruktúrou 3D MMI deliča 1×4 s PDMS ako obalovou vrstvou bolo možné túto štruktúru vyrobiť. Po optimalizácii dosiahla konečná štruktúra deliča celkovú dĺžku 459 µm.

V rámci spoločného bilaterálneho projektu so Žilinskou Univerzitou bol navrhnutý MMI delič 1×4 v 3D konfigurácii spolu s podpornou mechanickou konštrukciou vyrobený v dvoch krokoch pomocou komerčného zariadenia Nanoscribe Photonic Professional GT. Toto zariadenie používa jednostupňový proces založený na systéme priameho laserového zápisu (DLW z angl. direct laser wrtiting) a nelineárneho optického procesu dvojfotónovej polymerizácie (2PP z angl. two photon polymerization). Delenie optického signálu v tomto deliči sa overilo mikroskopickým meraním blízkeho poľa (NSOM z angl. near-field optical microscopy).

Variabilita MMI deliča v 3D konfigurácii sa overila aj zmenou konštrukcie MMI časti zo štvorcového prierezu na obdĺžnikový prierez s cieľom rozdeliť signál do šestich výstupov. Na základe zmeny prierezu MMI časti bol navrhnutý 3D MMI optický delič 1×6, ktorý bol opäť technologicky realizovaný na Žilinskej univerzite. Namerané a nasimulované výsledky 3D MMI deliča 1×6 potvrdili rozdelenie 1:6 s prítomnosťou slabého vyššieho módu vo vlnovodoch.

Prvky na báze nitridu kremíka pre medicínske aplikácie

Táto časť práce bola venovaná návrhu pasívnych optických deličov na báze nitridu kremíka. V tomto prípade je index lomu jadra vlnovodu $n_c = 1.925$ a index lomu obalu je $n_{cl} = 1.4575$. Prierez jadra vlnovodu je (0.8×0.16) µm^2. Deliče boli navrhnuté pre vlnovú dĺžku 850 nm. V tomto prípade sa ukazuje, ako materiál významne ovplyvňuje rozmery fotonických štruktúr. V porovnaní s klasickými štruktúrami na báze oxidu kremíka na kremíku bola ich dĺžka niekoľkokrát menšia a mali rovnako dobré optické vlastnosti. Tieto štruktúry sú teda vhodným kandidátom na miniaturizáciu a integráciu na čipe v novej, postupne sa rozvíjajúcej oblasti biofotonických alebo medicínskych aplikácií.

Najprv bol navrhnutý jednoduchý Y-delič 1 × 8, ktorého vložné straty dosiahli IL = -9.37 dB s nerovnomernosťou rozloženia optického signálu ILu = 0.68 dB pre TE polarizáciu. Vložné straty pre TM polarizáciu boli takmer rovnaké, a to IL = -9.95 dB s mierne vyššou nerovnomernosťou rozloženia optického signálu ILu = 0.98 dB. Výsledná veľkosť navrhnutého Y-deliča bola (840 × 28) µm^2.

Následne bol navrhnutý MMI delič 1 × 8, ktorý mal veľkosť (564 × 28) µm^2. MMI delič 1 × 8 bol ďalej optimalizovaný na základe limitácií technologického procesu dostupného v MLC CVTI SR Bratislava. Pri zohľadnení týchto limitácií bolo nutné zväčšiť navrhnutú štruktúru optického MMI deliča. A to nasledovne: medzi vstupný lineárny vlnovod a MMI časť deliča bol pridaný vstupný vlnovod v arcus tvare s dvomi rozdielnymi offsetami (33 µm a 73 µm) a inverzná vlnovodná štruktúra. Vložné straty oboch navhnutých MMI deličov boli podobné, konkrétne vložné straty MMI deliča 1 × 8 so vstupným offsetom 33 µm boli IL = -9.72 dB a nerovnomernosť rozloženia optického signálu ILu = 0.24 dB pre TE polarizáciu. Pre TM polarizáciu boli vložné straty ILu = -9.54 dB a nerovnomernosť rozloženia optického signálu ILu = 0.13 dB. Veľkosť štruktúry dosiahla (1624 × 54) µm^2. Vložné straty MMI deliča 1 × 8 so vstupným offsetom 73 µm boli rovnaké pre obe polarizácie, IL = -9.84 dB. Líšila sa len nerovnomernosť rozloženia optického signálu pre TE polarizáciu, ILu = 0.07 dB a TM polarizáciu, ILu = 0.23 dB. Veľkosť štruktúry dosiahla (2824 × 94) µm^2. Pre tieto dve konfigurácie MMI deliča boli následne vyrobené fotolitografické masky.

V spolupráci s partnerom v rámci spoločného projektu boli deliče vyrobené v MLC CVTI SR Bratislava použitím PECVD metódy a vyrobená štruktúra bola charakterizovaná topologickými a optickými metódami. Parametre štruktúry boli analyzované pomocou digitálneho mikroskopu a boli porovnané s parametrami získanými pomocou mikroskopie atomárnych síl (AFM z angl. atomic force microscopy). Výsledky z AFM boli presnejšie a približovali sa

viac k navrhnutým hodnotám. Výsledky z AFM však poukazujú aj na nepresnosť výrobného procesu, konkrétne na príliš hlboké zaleptanie vlnovodnej štruktúry, ktoré by sa dalo upraviť skrátením času leptania a optimalizáciou fotolitografického procesu.

Bibliography

1. PASCHOTTA, Rüdiger. *Optical Fiber Communications* [https://www.rp-photonics.com/optical_fiber_communications.html/]. [N.d.]. Accessed: 2023-08-23.
2. FRÖHLICH, Bernd; DYNES, James F; LUCAMARINI, Marco; SHARPE, Andrew W; TAM, Simon W-B; YUAN, Zhiliang; SHIELDS, Andrew J. Quantum secured gigabit optical access networks. *Scientific reports*. 2015, vol. 5, no. 1, s. 1–7.
3. BINDHAIQ, Salem; SUPA, Abu Sahmah M; ZULKIFLI, Nadiatulhuda; MOHAMMAD, Abu Bakar; SHADDAD, Redhwan Q; ELMAGZOUB, Mohamed A; FAISAL, Ahmad, et al. Recent development on time and wavelength-division multiplexed passive optical network (TWDM-PON) for next-generation passive optical network stage 2 (NG-PON2). *Optical Switching and Networking*. 2015, vol. 15, s. 53–66.
4. MOUGHAMES, Johnny; PORTE, Xavier; THIEL, Michael; ULLIAC, Gwenn; LARGER, Laurent; JACQUOT, Maxime; KADIC, Muamer; BRUNNER, Daniel. Three-dimensional waveguide interconnects for scalable integration of photonic neural networks. *Optica*. 2020, vol. 7, no. 6, s. 640–646.
5. GONZÁLEZ-FERNÁNDEZ, AA; JUVERT, J; ACEVES-MIJARES, M; DOMÍNGUEZ, C. Monolithic integration of a silicon-based photonic transcei-ver in a CMOS process. *IEEE Photonics Journal*. 2015, vol. 8, no. 1, s. 1–13.
6. PHOTONDELTA. *Why Can Silicon Nitride Be an Ideal Platform for Photonic Integrated Circuits?* [https://www.photondelta.com/news/why-can-silicon-nitride-sin-be-ideal-platform-for-photonic-integrated-circuits/]. 2022. Accessed: 2023-08-23.
7. LEIJTENS, Xaveer Jm; KUHLOW, Berndt; SMIT, Meint K. Wavelength filters in fibre optics. *Arrayed Waveguide Gratings*. 2006, vol. 123, s. 125–187.
8. PARVATHI, Nair S; TRISNO, Jonathan; WANG, Hongtao; YANG, Joel KW. 3D printed fiber sockets for plug and play micro-optics. *International Journal of Extreme Manufacturing*. 2021, vol. 3, no. 1.
9. RIGHINI, Giancarlo C; FERRARI, Maurizio. *Integrated Optics: Characterization, devices, and applications, Volume 2*. Institution of Engineering and Technology, 2020.
10. MARTENS, Daan; RAMIREZ-PRIEGO, Patricia; MURIB, Mohammed Shariff; ELAMIN, Ayssar A; GONZÁLEZ-GUERRERO, Ana Belén; STEHR, M; JONAS, F; ANTON, Birgit; HLAWATSCH, N; SOETAERT, Pieterjan, et al. A low-cost integrated biosensing platform based on SiN nanophotonics for biomarker detection in urine. *Analytical methods*. 2018, vol. 10, no. 25, s. 3066–3073.
11. TYLER, Nicola A; FOWLER, Daivid; MALHOUITRE, Stephane; GARCIA, Stephanie; GROSSE, Philippe; RABAUD, Wilfried; SZELAG, Bertrand. SiN integrated optical phased arrays for two-dimensional beam steering at a single near-infrared wavelength. *Optics express*. 2019, vol. 27, no. 4, s. 5851–5858.
12. MARTENS, Daan; SUBRAMANIAN, Ananth Z; PATHAK, Shibnath; BROUCK, Michael Van-slem; BIENSTMAN, Peter; BOGAERTS, Wim; BAETS, Roel G. Compact silicon nitride arrayed waveguide gratings for very near-infrared wavelengths. *IEEE Photonics Technology Letters*. 2014, vol. 27, no. 2, s. 137–140.
13. POENAR, Daniel Puiu. Microfluidic and micromachined/MEMS devices for separation, discrimination and detection of airborne particles for pollution monitoring. *Micromachines*. 2019, vol. 10, no. 7, s. 483.
14. PELTOMAA, Riikka; GLAHN-MARTÍNEZ, Bettina; BENITO-PEÑA, Elena; BONDI-MORENO, María C. Optical biosensors for label-free detection of small molecules. *Sensors*. 2018, vol. 18, no. 12, s. 4126.
15. ROMERO-GARCÍA, Sebastian; KLOS, Thomas; KLEIN, Edwin; LEUERMANN, Jonas; GEUZEBROEK, Douwe; KERKHOF, Joost van; BÜSCHER, Martin; KRIEG,

Jürgen; LEISCHING, Patrick; WITZENS, Jeremy. Photonic integrated circuits for multi-color laser engines. In: *Silicon Photonics XII*. SPIE, 2017, vol. 10108, s. 178–188.
16. MASHAYEKH, Alireza T; KLOS, Thomas; KOCH, Sina; MERGET, Florian; GEUZEBROEK, Douwe; KLEIN, Edwin; VEENSTRA, Theo; BÜSCHER, Martin; LEISCHING, Patrick; WITZENS, Jeremy. Miniaturized PIC multi-color laser engines for the life sciences. In: *Smart Photonic and Optoelectronic Integrated Circuits XXI*. SPIE, 2019, vol. 10922, s. 137–148.
17. BAETS, Roel. Silicon-Photonics-Based Spectroscopic Sensing for Environmental Monitoring and Health Care. In: *2021 Optical Fiber Communications Conference and Exhibition (OFC)*. IEEE, 2021, s. 1–42.
18. BURTSCHER, Catalina; SEYRINGER, Dana; UHEREK, Frantisek; CHO-VAN, Jozef; KUZMA, Anton. Design of low loss 1× 64 y-branch splitter having symmetric splitting ratio and small footprint. In: *The Tenth International Conference on Advanced Semiconductor Devices and Microsystems*. IEEE, 2014, s. 1–4.
19. AGALLIU, Rajdi; BURTSCHER, Catalina; LUCKI, Michal; SEYRINGER, Dana. Optical splitter design for telecommunication access networks with triple-play services. *Journal of Electrical Engineering*. 2018, vol. 69, no. 1, s. 32–38.
20. SERECUNOVA, Stanislava; SEYRINGER, Dana; UHEREK, Frantisek; SEYRINGER, Heinz. Waveguide shape and waveguide core size optimization of Y-branch optical splitters up to 128 splitting ratio. *Optics Communications*. 2021, vol. 501, s. 127362.
21. CHAUDHARI, Chitrarekha; PATIL, Dnyaneshwar S; GAUTAM, DK. A new technique for the reduction of the power loss in the Y-branch optical power splitter. *Optics communications*. 2001, vol. 193, no. 1-6, s. 121–125.
22. KOHLER, L. Study of the optical properties of passive optical splitters based on MMI and Y-branch approach. *Vorarlberg University of Applied Science, Austria, master thesis*. 2012.
23. WANG, Liangliang; AN, Junming; ZHANG, Jiashun; WU, Yuanda; LI, Jianguang; WANG, Hongjie; WANG, Yue; PAN, Pan; ZHONG, Fei; ZHA, Qiang, et al. Design and fabrication of optical power splitters with large port count. *Chinese Optics Letters*. 2014, vol. 12, no. 9, s. 092302.
24. SERECUNOVA, Stanislava; SEYRINGER, Dana; UHEREK, Frantisek; SEYRINGER, Heinz. Design and optimization of optical power splitters for optical access networks. *Optical and Quantum Electronics*. 2022, vol. 54, no. 6, s. 365.
25. SERECUNOVA, Stanislava; SEYRINGER, Dana; UHEREK, Frantisek; SEYRIGER, Heinz. Comparison of optical properties of 1x128 splitters based on Y-branch and MMI approaches. In: *Optical Components and Materials XVIII*. SPIE, 2021, vol. 11682, s. 230–237.
26. RASMUSSEN, Thomas; RASMUSSEN, Jesper Kiel; POVLSEN, Jorn Hedegaard. Design and performance evaluation of 1-by-64 multimode interference power splitter for optical communications. *Journal of lightwave technology*. 1995, vol. 13, no. 10, s. 2069–2074.
27. GAŠO, Peter; PUDIŠ, Dušan; SEYRINGER, Dana; KUZMA, Anton; GAJDOŠOVÁ, Lenka; MIZERA, Tomáš; GORAUS, Matej. 3D polymer based 1x4 beam splitter. *Journal of Lightwave Technology*. 2020, vol. 39, no. 1, s. 154–161.
28. SERECUNOVA, Stanislava; SEYRINGER, Dana; SEYRINGER, Heinz; UHEREK, Frantisek; MIZERA, Tomas; PUDIS, Dusan. Design and simulation of polymer based 1x4 multimode interference splitter. In: *AIP Conference Proceedings*. AIP Publishing, 2021, vol. 2411. No. 1.
29. SERECUNOVA, Stanislava; SEYRINGER, Dana; PUDIS, Dusan; MIZERA, Tomas; UHEREK, Frantisek; SEYRINGER, Heinz. Design and simulation of 3D 1× 4 multimode interference splitter. In: *2022 International Conference on Broadband Com-*

munications for Next Generation Networks and Multimedia Applications (CoBCom). IEEE, 2022, s. 1–5.

30. GAJDOSOVA, Lenka; SEYRINGER, Dana; GAŠO, Peter; JANDURA, Daniel; PUDIŠ, Dušan. Design, simulation and technological realization of polymer based 3D 1x4 splitter. In: *AIP Conference Proceedings*. AIP Publishing LLC, 2019, vol. 2131, s. 020012. No. 1.
31. SERECUNOVA, Stanislava; MIZERA, Tomas; SEYRINGER, Dana; PUDIS, Dusan; UHEREK, Frantisek; SEYRINGER, Heinz. 3D Polymer Based 1×4 Multimode Interference Splitter. In: *2023 23rd International Conference on Transparent Optical Networks (ICTON)*. 2023, s. 1–4. Dostupné z DOI: 10.1109/ICTON59386.2023.10207511.
32. SERECUNOVA, Stanislava; SEYRINGER, Dana; MIZERA, Tomas; PUDIS, Dusan; UHEREK, Frantisek; SEYRINGER, Heinz. Comparison of 3D 1x4 splitters based on different splitting approaches. In: *Proceedings of ADEPT 2022. 10th International Conference on Advances in Electronic and Photonic Technologies. Tatranská Lomnica (SK), 20.06. 2022-24.06. 2022*. University of Zilina in EDIS-Publishing Centre of UZ, [n.d.], s. 105–108.
33. KATEDRA FYZIKA, FEIT UNIZA. *Oddelenie optiky a fotoniky* [https://fyzika.uniza.sk/oddelenie-optiky-a-fotoniky/]. 2023. Accessed: 2023-08-23.
34. NANOSCRIBE PHOTONICS PROFESIONAL GT2. *World's highest resolution 3D printer* [https://www.nanoscribe.com/en/products/photonic-professional-gt2/?gclid=CjOKCQjwiIOmBhDjARIsAP6YhSUkNsVNTOqzpfXAdAf_K5HoqG7ggFbLRLD2KpvYgHGTUUfyDXWVyPkaAo7_EALw_wcB]. Nanoscribe GmbH Co. KG, 2023. Accessed: 2023-07-26.
35. SERECUNOVA, Stanislava; MIZERA, Tomas; SEYRINGER, Dana; PUDIS, Dusan; UHEREK, Frantisek; SEYRINGER, Heinz. Polymer-based 3D 1x6 MMI coupler. In: *Proceedings of ADEPT 2023. 11th International Conference on Advances in Electronic and Photonic Technologies. Podbanské (SK), 2023-12.-15.06. 2023*. University of Zilina in EDIS-Publishing Centre of UZ, [n.d.], 221—224.
36. INTERNATIONAL LASER CENTRE. *International Laser Centre of SCSTI* [http://www.ilc.sk/en/]. 2023. Accessed: 2023-05-30.
37. SEYRINGER, Dana; SAGMEISTER, Martin; MAESE-NOVO, Alejandro; EGGELING, Moritz; RANK, E; MUELLNER, Paul; HAINBERGER, Rainer; DREXLER, Wolfgang; VLASKOVIC, Marko; ZIMMERMANN, Horst, et al. Technological verification of size-optimized 160-channel silicon nitride-based AWG-spectrometer for medical applications. *Applied Physics B*. 2019, vol. 125, s. 1–10.
38. SERECUNOVA, Stanislava; SEYRINGER, Dana; UHEREK, Frantisek; CHOVAN, Jozef; SEYRINGER, Heinz. Comparison of optical properties of 1× 8 Y-branch and MMI splitter based on silicon nitride material platform. In: *22nd Polish-Slovak-Czech Optical Conference on Wave and Quantum Aspects of Contemporary Optics*. SPIE, 2022, vol. 12502, s. 83–89.
39. KÖFFERLEIN, Matthias. *Klayout* [https://www.klayout.de/]. 2020. Accessed: 2023-06-26.
40. SLOVAK UNIVERSITY OF TECHNOLOGY. *Institute of Electronics and Photonics* [https://www.fei.stuba.sk/english/institutes-and-departments/institute-of-electronics-and-photonics.html?page_id=3638]. 2020. Accessed: 2023-08-24.
41. CHOVAN, J; FIGURA, D; CHLPÍK, J; LORENC, D; ŘEHÁČEK, V; UHEREK, F. Design, fabrication and characterization of SiOx/SiON/SiO2/Si structures for passive optical waveguides realization. In: *Photonics, Devices, and Systems VII*. SPIE, 2017, vol. 10603, s. 139–145.
42. ZEISS, Research Microscopy Solutions. *ZEISS Axioscope 5* [https://www.zeiss.com/microscopy/de/produkte/lichtmikroskope/weitfeldmikroskope/axioscope-5.html#countrySwitch]. 2023. Accessed: 2023-08-24.

A. List of author's publications

1. Category A+, A, A- and B outputs: total: 36
2. Category A+ and A outputs: total: 2
3. Number of publications in WoS/SCOPUS: total 25 (of which 8 in WoS and 17 in SCOPUS)

Category A+: 2

V3 Scientific output of journal publications

1. **Stanislava Serecunova** [75 %], Dana Seyringer [10 %], Frantisek Uherek [10 %], Heinz Seyringer [5 %]. "Design and optimization of optical power splitters for optical access networks". In: *Optical and Quantum Electronics* 54.6 (2022), p. 365. (2022: 3.000 - IF, Q2 - JCR Best Q, 0.433 - SJR, Q2 - SJR Best Q). In the database: SCOPUS: 2-s2.0-85130220886; WOS: 000796994300001; CC: 000796994300001; DOI: 10.1007/s11082-022-03620-z.
Publication category until 2021: ADC
2. **Stanislava Serecunova** [75 %], Dana Seyringer [10 %], Frantisek Uherek [10 %], Heinz Seyringer [5 %]. "Waveguide shape and waveguide core size optimization of Y-branch optical splitters up to 128 splitting ratio". In: *Optics Communications* 501 (2021), p. 127362. (2021: 2.335 - IF, Q3 - JCR Best Q, 0.589 - SJR, Q2 - SJR Best Q). In CC database: 000696943300009; WOS: 000696943300009; SCOPUS: 2-s2.0-85114665064; DOI: 10.1016/j.optcom.2021.127362.
Publication category until 2021: ADC

Category A-: 18

3. **Stanislava Serečunová** [80 %], Dana Seyringer [10 %], Frantisek Uherek [5 %], Heinz Seyringer [5 %]. "Design and optimization of 1×2 N Y-branch optical splitters for telecommunication applications". In: *Journal of Electrical Engineering* 71.5 (2020), pp. 353–358. (2020: 0.647 - IF, Q4 - JCR Best Q, 0.191 - SJR, Q3 - SJR Best Q). In the database: DOI: 10.2478/jee-2020-004; WOS: 000595157800008; SCOPUS: 2-s2.0-85097559285.
Publication category to 2021: ADN

V2 Scientific publication output as part of an edited book or proceedings

4. **Stanislava Serecunova** [45 %], Tomas Mizera [15 %], Dana Seyringer [15 %], Dusan Pudis [10 %], Frantisek Uherek [10 %], Heinz Seyringer [5 %]. "3D Polymer Based 1×4 Multimode Interference Splitter". In: *23rd International Conference on Transparent Optical Networks (ICTON)*. Bucharest, Romania, 2023, pp. 1-4. In the database: IEEE: 10207511; DOI: 10.1109/ICTON59386.2023.10207511.
Publication category to 2021: AFC

5. Dana Seyringer [40 %], **Stanislava Serecunova** [35 %], Frantisek Uherek [15 %], Heinz Seyringer [5 %], Jozef Chovan [5 %]. "256 Channel 10 GHz AWG Demultiplexer for Ultra Dense WDM". In: *23rd International Conference on Transparent Optical Networks (ICTON)*. Bucharest, Romania, 2023, pp. 1-4. In the database: IEEE: 10207508; DOI: 10.1109/ICTON59386.2023.10207508.
Publication category to 2021: AFC

6. **Stanislava Serecunova** [65 %], Dana Seyringer [10 %], Frantisek Uherek [10 %], Jozef Chovan [10 %], Heinz Seyringer [5 %]. "Comparison of optical properties of 1×8 Y-branch and MMI splitter based on silicon nitride material platform". In: *22nd Polish-Slovak-Czech Optical Conference on Wave and Quantum Aspects of Contemporary Optics*. Vol. 12502. SPIE. 2022, pp. 83–89. (2022: 0.166 - SJR). In the database: DOI: 10.1117/12.2662002; WOS: 000920988700014; SCOPUS: 2-s2.0-85145357509.
Publication category to 2021: AFC

7. Dusan Pudis [30 %], Tomas Mizera [25 %], Peter Gaso [20 %], Martin Ziman [10 %], **Stanislava Serecunova** [10 %], Dana Seyringer [5 %]. "3D MMI optical splitter with output waveguides and its near-field characterization". In: *22nd Polish-Slovak-Czech Optical Conference on Wave and Quantum Aspects of Contemporary Optics*. Vol. 12502. SPIE. 2022, pp. 136–140. (2022: 0.166 - SJR). In the database: DOI: 10.1117/12.2664188; SCOPUS: 2-s2.0-85145349654; WOS: 000920988700023.
Publication category to 2021: AFC

8. Dana Seyringer [40 %], **Stanislava Serecunova** [35 %], Frantisek Uherek [20 %], Heinz Seyringer [5 %]. "Design of 256-channel 25-GHz AWG for ultradense wavelength division multiplexing". In: *22nd Polish-Slovak-Czech Optical Conference on Wave and Quantum Aspects of Contemporary Optics*. Vol. 12502. SPIE. 2022, pp. 95–100. (2022: 0.166 - SJR). In the database: DOI: 10.1117/12.2663317; SCOPUS: 2-s2.0-85145359560; WOS: 000920988700016.
Publication category to 2021: AFC

9. **Stanislava Serecunova** [55 %], Dana Seyringer [10 %], Dusan Pudis [10 %], Tomas Mizera [10 %], Frantisek Uherek [10 %], Heinz Seyringer [5 %]. "Design and simulation of 3D 1×4 multimode interference splitter". In: *2022 International Conference on Broadband Communications for Next Generation Networks and Multimedia Applications (CoBCom)*. IEEE. 2022, pp. 1–5. In the database: DOI: 10.1109/CoBCom55489.2022.9880770; SCOPUS: 2-s2.0-85139421206; IEEE: 9880770.
Publication category to 2021: AFC

10. Manuel Humpeler [50 %], **Stanislava Serecunova** [25 %], and Dana Seyringer [25 %]. "AWG-Channel-Spacing: A new software tool to calculate accurate channel spacing of an AWG optical multiplexer/demultiplexer". In: *2022 International Conference on Broadband Communications for Next Generation Networks and Multimedia Applications (CoBCom)*. IEEE. 2022, pp. 1–5. In the database: DOI: 10.1109/CoBCom55489.2022.9880652; SCOPUS: 2-s2.0-85139455037; IEEE: 9880652.
Publication category to 2021: AFC

11. Severin Keller [30 %], Dusko Vukovic [25 %], **Stanislava Serecunova** [20 %], Dana Seyringer [20 %], Fiorentino Valerio Conte [5 %]. "AWG-Wuckler: A novel software tool for flexible design of arrayed waveguide gratings". In: *2022 International Conference on Broadband Communications for Next Generation Networks and Multimedia Applications (CoBCom)*. IEEE. 2022, pp. 1–6. In the database: DOI: 10.1109/CoBCom55489.2022.9880624; SCOPUS: 2-s2.0-85139382835; IEEE: 9880624.
Publication category to 2021: AFC

12. **Stanislava Serecunova** [80 %], Dana Seyringer [10 %], Frantisek Uherek [5 %], Heinz Seyringer [5 %]. "Comparison of optical properties of 1x128 splitters based on Y-branch and MMI approaches". In: *Optical Components and Materials*

XVIII. Vol. 11682. International Society for Optics and Photonics. 2021, 116821N. In the database: SCOPUS: 2-s2.0-85105910983; WOS: 000703947800030; DOI: 10.1117/12.2582994.
Publication category to 2021: AFC

13. Dana Seyringer [30 %], **Stanislava Serecunova** [30 %], Heinz Seyringer [20 %], Frantisek Uherek [20 %]. "Impact of phased array on optical performance of AWG-spectrometers". In: *Frontiers in Optics*. Optica Publishing Group. 2020, JTh4B–13. In the database: SCOPUS: 2-s2.0-85105981348.
Publication category to 2021: AFC

14. Johann Zehetner [15 %], Dana Seyringer [10 %], Fadi Dohnal [10 %], **Stanislava Serecunova** [10 %], Heinz Seyringer [5 %], Ivan Hotovy [10 %], Miroslav Mikulasek [10 %], Peter Ondrejka [10 %], Juraj Hotovy [10 %], Vlastimil Rehacek [10 %]. "AWG-Spectrometer to Analyze Absorption Spectra of Optical Gas Sensors Fabricated by Femtosecond Laser Processing". In: *28th International Conference Applied Physics of Condensed Matter*. June 2023. (will be published in AIP Conference Proceedings).
Publication category until 2021: AFD

15. Jozef Chovan [75 %], Frantisek Uherek [5 %], Martin Tomaška [5 %], **Stanislava Serecunova** [5 %], Dana Seyringer [5 %], Heinz Seyringer [5 %]. "Optimization of 2x2 optical switch based on MMI splitters by using waveguide tapers". In: *2022 14th International Conference on Advanced Semiconductor Devices and Microsystems (ASDAM)*. IEEE. 2022, pp. 1–4. In the database: DOI: 10.1109/ASDAM55965.2022.9966794; IEEE: 9966794; SCOPUS: 2-s2.0-85144590916.
Publication category until 2021: AFD

16. Dusan Pudis [25 %], Tomas Mizera [20 %], Peter Gaso [15 %], Anton Kuzma [10 %], Martin Ziman [10 %], **Stanislava Serecunova** [10 %], Dana Seyringer [5 %], Matej Goraus [5 %]. "3D optical splitters based on polymers". In: *2022 14th International Conference on Advanced Semiconductor Devices and Microsystems (ASDAM)*. IEEE. 2022, pp. 1–4. In the database: DOI: 10.1109/ASDAM55965.2022.9966741; IEEE: 9966741; SCOPUS: 2-s2.0-85144592537.
Publication category until 2021: AFD

17. **Stanislava Serecunova** [55 %], Dana Seyringer [10 %], Dusan Pudis [10 %], Tomas Mizera [10 %], Frantisek Uherek [10 %], Heinz Seyringer [5 %]. "Optimization of 3D 1×4 multimode interference splitter based on polymer material platform". In: *AIP Conference Proceedings*. Vol. 2778. 1. AIP Publishing LLC. 2023, p. 030009. In the database: DOI: 10.1063/5.0135780; SCOPUS: 2-s2.0-85160269189.
Publication category until 2021: AFD

18. Dana Seyringer [35 %], **Stanislava Serečunová** [25 %], Peter Gašo [10 %], Dušan Pudiš [10 %], Heinz Seyringer [5 %], František Uherek [5 %], Fadi Dohnal [5 %], Johann Zehetner [5 %]. "Design of 16-channel, 100-GHz multimode polymer-based AWG". *AIP Conference Proceedings*. Vol. 2778. 1. AIP Publishing LLC. 2023. p. 030010. In the database: DOI: 10.1063/5.0136128 ; SCOPUS: 2-s2.0-85160271575.
Publication category until 2021: AFD

19. Tomáš Mizera [40 %], Dusan Pudis [10 %], Anton Kuzma [15 %], Dana Seyringer [5 %], Peter Gaso [20 %], Patrik Micek [5 %], **Stanislava Serecunova** [5 %]. "3D Optical Splitter based on MMI". In: *Transportation Research Procedia*. 55 (2021), pp. 949–954. In the database: SCOPUS: 2-s2.0-85112610619; DOI: 10.1016/j.trpro.2021.07.181.
Publication category until 2021: AFD

20. **Stanislava Serecunova** [65 %], Dana Seyringer [10 %], Heinz Seyringer [5 %], Frantisek Uherek [10 %], Tomas Mizera [5 %], Dusan Pudis [5 %]. "Design and simulation of polymer based 1x4 multimode interference splitter". In: *AIP Conference*

Proceedings. Vol. 2411. 1. AIP Publishing LLC. 2021, p. 060004. In the database: DOI: 10.1063/5.0067344; SCOPUS: 2-s2.0-85118864880; WOS: 000859097600029.
Publication category until 2021: AFD

Category B: 16

21. **Stanislava Serecunova** [40 %], Tomas Mizera [25 %], Dana Seyringer [10 %], Dusan Pudis [10 %], Frantisek Uherek [10 %], Heinz Seyringer [5 %]. "Polymer-based 3D 1x6 MMI coupler". In: *Proceedings of ADEPT. 11th International Conference on Advances in Electronic and Photonic Technologies*. University of Zilina in EDIS-Publishing Centre of UZ, 2023, pp. 221–224. ISBN: 978-80-554-1977-0.
Publication category until 2021: AFD

22. Jozef Chovan [80 %], Frantisek Uherek [5 %], Martin Tomaška [5 %], **Stanislava Serecunova** [5 %], Dana Seyringer [5 %]. "Characterization of photonics devices by coherent optical frequency domain reflectometry". In: *Proceedings of ADEPT. 11th International Conference on Advances in Electronic and Photonic Technologies*. University of Zilina in EDIS-Publishing Centre of UZ, 2023, pp. 146–149. ISBN: 978-80-554-1977-0.
Publication category until 2021: AFD

23. Tomáš Mizera [30 %], Peter Gaso [30 %], Patrik Micek [15 %], **Stanislava Serecunova** [15 %], Daniel Jandura [5 %], Dusan Pudis [5 %]. "Polymer based 3D 1x4 MMI coupler with branched output waveguides". In: *Proceedings of ADEPT. 11th International Conference on Advances in Electronic and Photonic Technologies*. University of Zilina in EDIS-Publishing Centre of UZ, 2023, pp. 193–197. ISBN: 978-80-554-1977-0.
Publication category until 2021: AFD

24. **Stanislava Serecunova** [55 %], Dana Seyringer [10 %], Tomas Mizera [10 %], Dusan Pudis [10 %], Frantisek Uherek [10 %], Heinz Seyringer [5 %]. "Comparison of 3D 1x4 splitters based on different splitting approaches". In: *Proceedings of ADEPT. 10th International Conference on Advances in Electronic and Photonic Technologies*. University of Zilina in EDIS-Publishing Centre of UZ, 2022, pp. 105–108. ISBN: 978-80-554-1884-1.
Publication category until 2021: AFD

25. Jozef Chovan [80 %], Frantisek Uherek [5 %], Martin Tomaska [5 %], **Stanislava Serecunova** [5 %], Dana Seyringer [5 %]. "Design and modeling of 2x2 optical switch". In: *Proceedings of ADEPT. 10th International Conference on Advances in Electronic and Photonic Technologies*. University of Zilina in EDIS-Publishing Centre of UZ, 2022, pp. 185–188. ISBN: 978-80-554-1884-1.
Publication category until 2021: AFD

26. Dana Seyringer [40 %], **Stanislava Serecunova** [25 %], Jozef Chovan [10 %], Fadi Dohnal [10 %], Frantisek Uherek [10 %], Heinz Seyringer [5 %]. "Influence of Rib Waveguides on Performance of SiN-Based AWGs". In: *Proceedings of ADEPT. 10th International Conference on Advances in Electronic and Photonic Technologies*. University of Zilina in EDIS-Publishing Centre of UZ, 2022, pp. 181–184. ISBN: 978-80-554-1884-1.
Publication category until 2021: AFD

27. **Stanislava Serecunova** [25 %], Dana Seyringer [25 %], Frantisek Uherek [25 %], Heinz Seyringer [25 %]. "Influence of different shapes of output waveguides on optical performance of 1x128 multimode interference splitter". In: *Proceedings of ADEPT. 9th International Conference on Advances in Electronic and Photonic Technologies*.

University of Zilina in EDIS-Publishing Centre of UZ, 2021, pp. 239–242. ISBN: 978-80-554-1806-3.
Publication category until 2021: AFD

28. Jozef Chovan [10 %], Frantisek Uherek [10 %], Martin Tomaska [10 %], Lubos Podlucky [35 %], Eduard Koza [5 %], Jozef Pavlov [5 %], **Stanislava Serecunova** [20 %], Dana Seyringer [5 %]. "Temperature characterization of fiber array to photonics chip coupling". In: *Proceedings of ADEPT. 9th International Conference on Advances in Electronic and Photonic Technologies*. University of Zilina in EDIS-Publishing Centre of UZ, 2021, pp. 21–24. ISBN: 978-80-554-1806-3.
Publication category until 2021: AFD

29. Johann Zehenzer [20 %], Dana Seyringer [20 %], **Stanislava Serecunova** [15 %], Peter Gaso [10 %], Dusan Pudis [10 %], Ivan Hotovy [10 %], Miroslav Mikolasek [10 %], Heinz Seyringer [5 %]. "Fabrication of passive and active photonics coupling structures using fs-laser ablation". In: *Proceedings of ADEPT. 9th International Conference on Advances in Electronic and Photonic Technologies*. University of Zilina in EDIS-Publishing Centre of UZ, 2021, pp. 255–258. ISBN: 978-80-554-1806-3.
Publication category until 2021: AFD

30. Dana Seyringer [20 %], **Stanislava Serecunova** [30 %], Heinz Seyringer [10 %], Johann Zehenzer [10 %], Tomas Mizera [10 %], Dusan Pudis [10 %], Frantisek Uherek [10 %]. "Design of 16-channel, 100-GHz polymer-based AWG". In: *Proceedings of ADEPT. 9th International Conference on Advances in Electronic and Photonic Technologies*. University of Zilina in EDIS-Publishing Centre of UZ, 2021, pp. 243–246. ISBN: 978-80-554-1806-3.
Publication category until 2021: AFD

31. Dana Seyringer [30 %], **Stanislava Serecunova** [25 %], Frantisek Uherek [20 %], Jozef Chovan [15 %], Dusan Pudis [5 %], Heinz Seyringer [5 %]. "Arrayed waveguide gratings for photonics applications". In: *INTERPHOTICS 2021 Abstract Book*. Gebze Teknik University, 2021, p. 14.
Publication category until 2021: AFE

32. Jozef Chovan [65 %], Frantisek Uherek [5 %], Martin Tomaska [5 %], Eduard Koza [5 %], Jozef Pavlov [5 %], **Stanislava Serecunova** [5 %], Dana Seyringer [5 %]. "Temperature stability of fiber array to photonics chip butt coupling". In: *INTERPHOTICS 2021 Abstract Book*. Gebze Teknik University, 2021, pp. 16–17.
Publication category until 2021: AFE

33. Dana Seyringer [30 %], **Stanislava Serecunova** [30 %], Jozef Chovan [20 %], Frantisek Uherek [20 %]. "Impact of different waveguide structures on optical properties of SiN based AWG-spectrometers". In: *14th International Conference on Advanced Semiconductor Devices and Microsystems*. 2022.
Publication category until 2021: AFH

34. **Stanislava Serecunova** [75 %], Dana Seyringer [10 %], Frantisek Uherek [10 %], Heinz Seyringer [5 %]. "Design of 1×8 multimode interference splitter based on SiN material platform". In: *Extended Abstract Book of 7th conference SURFINT-SREN VII*. Comenius University, Bratislava, Slovakia, 2021, pp. 55–56. ISBN: 978-80-223-5296-3.
Publication category until 2021: AFH

35. Dana Seyringer [40 %], **Stanislava Serecunova** [30 %], Frantisek Uherek [30 %]. "Optical MUX/ DeMUX for Telecom Applications". In: *26th International conference on applied physics of condensed matter*. 2021.
Publication category until 2021: AFH

O2 Scientific publication output as part of a book publication or proceedings paper from an event

36. Tomas Mizera [20 %], Dusan Pudis [20 %], Peter Gaso [20 %], Anton Kuzma [15 %], Patrik Micek [10 %], Dana Seyringer [5 %], **Stanislava Serecunova** [10 %]. "Optical 1:9 splitter based on MMI, prepared by 3D litography". In: *Book of Abstracts of the 22nd Polish-Slovak-Czech Optical Conference on Wave and Quantum Aspects of Contemporary Optics*. Department of Optics, Photonics, Faculty of Fundamental Problems of Technology, Wroclaw University of Science, and Technology, 2021, p. 137.
Publication category until 2021: BFA

Statistics: publication category from 2022

V3	Scientific publication output as part of an edited book or proceedings	3
V2	Scientific output of journal publications	32
O2	Scientific publication output as part of a book publication or proceedings paper from an event	1
Summary		**36**

Statistics: publication category until 2021

ACD	Scientific papers in foreign journals with impact factor	2
ADN	Scientific papers in domestic journals registered in Web of Science or SCOPUS databases	1
AFC	Published papers at foreign scientific conferences	10
AFD	Published papers at domestic scientific conferences	17
AFE	Abstract of invited papers from foreign scientific conferences	2
AFH	Abstract of papers from domestic scientific conferences	3
BFA	Abstracts of professional papers from foreign events (conferences...)	1
Summary		**36**

B. References to the author´s publications

Publication:
Stanislava Serecunova, Dana Seyringer, Frantisek Uherek, Heinz Seyringer. "Design and optimization of optical power splitters for optical access networks". In: *Optical and Quantum Electronics* 54.6 (2022), p. 365.

Cited in:

1. Raquel Fernández de Cabo, Jaime Vilas, Pavel Cheben, Aitor Velasco, David González-Andrade. "Experimental characterization of an ultra-broadband dual-mode symmetric Y–junction based on metamaterial waveguides". In: *Optics and Laser Technology* 157 (2023), p. 108742.

2. Lila Mokhtari, Hadjira Badaoui, Mehadji Abri, Bachir Rahmi, Farah Lallam, Abdelbasset Moungar. "Efficient 1×2, 1×4, 1×8 and 1×16 photonic crystal filters/power splitters based ring resonators for modern passive optical network PON". In: *Modern Physics Letters B* Vol. 37, No. 22 (2023), p. 2350064.

Publication:
Stanislava Serecunova, Dana Seyringer, Frantisek Uherek, Heinz Seyringer. "Waveguide shape and waveguide core size optimization of Y-branch optical splitters up to 128 splitting ratio". In: *Optics Communications* 501 (2021), p. 127362.

Cited in:

1. Yu Zheng, Lianqiong Jiang, Jie Cheng, Jianzhe Liu, Ji'an Duan. "Experimental Research on In Situ Uniaxial Tensile Response of Silica-Based PLC Optical Splitters". In: *Applied Sciences* 12.12 (2022), p. 5778.

2. Nauval Franata, Retno Wigajatri Purnamaningsih. "Design of a 1x4 optical power divider based on Y-branch using III-nitride semiconductor". In: *Jurnal Ilmiah Teknik Elektro Komputer dan Informatika* 8.1 (Apr. 2022), p. 119.

3. Tomas Mizera. "3D fotonické prvky pre aplikácie na cipe". In: Dissertation thesis, *University of Zilina, Faculty of Electrical Engineering and Information Technology* (2022), p.25.

Publication:
Stanislava Serečunová, Dana Seyringer, Frantisek Uherek, Heinz Seyringer. "Design and optimization of 1×2 N Y-branch optical splitters for telecommunication applications". In: *Journal of Electrical Engineering* 71.5 (2020), pp. 353–358.

Cited in:

1. Yuting Xu, Zhongxing Tian, Xiaoqin Meng, Zhen Chai. "Methods and applications of on-chip beam splitting: A review". In: *Front. Phys.* 10 (Sept. 2022).

Publication:
Stanislava Serecunova, Dana Seyringer, Frantisek Uherek, Heinz Seyringer. "Comparison of optical properties of 1x128 splitters based on Y-branch and MMI approaches". In: *Optical Components and Materials XVIII*. Vol. 11682. International Society for Optics and Photonics. (2021), 116821N.

Cited in:

1. Liangliang Wang, Bingli Sun, Jiashun Zhang, Junming An, Jianguang Li, Xiaojie Yin, Jun Chen, Xiasen Chang, Yuanda Wu. "Low-loss 1×256 optical power splitter". In: Optical Engineering 60.12 (2021), pp. 127102–127102.

2. MD Rasel et al. "Step and graded-index core-based polymer multimode interference splitters for photonic integrated circuits". In: *Optica Open.* (2023).

Publication:
Tomáš Mizera, Dusan Pudis, Anton Kuzma, Dana Seyringer, Peter Gaso, Patrik Micek, Stanislava Serecunova. "3D Optical Splitter based on MMI". In: *Transportation Research Procedia.* 55 (2021), pp. 949–954.

Cited in:

1. Yuting Xu, Zhongxing Tian, Xiaoqin Meng, Zhen Chai. "Methods and applications of on-chip beam splitting: A review". In: *Front. Phys.* 10 (Sept. 2022).

2. Martin Ziman, Martin Feiler, Tomas Mizera, Anton Kuzma, Dusan Pudis, Frantisek Uherek. "Design of a Power Splitter Based on a 3D MMI Coupler at the Fibre-Tip". In: Electronics 11.18 (2022), p. 2815.

Publication:
Jozef Chovan, Frantisek Uherek, Martin Tomaška, **Stanislava Serecunova**, Dana Seyringer, Heinz Seyringer. "Optimization of 2×2 optical switch based on MMI splitters by using waveguide tapers". In: *2022 14th International Conference on Advanced Semiconductor Devices and Microsystems (ASDAM).* IEEE. 2022, pp. 1–4.

Cited in:

1. Abdul Razak, Hanim, et al. "Modelling Of Different Tapered Structures of Multimode Interference (MMI) Couplers". Przeglad Elektrotechniczny 99.7 (2023).

Citations: 11 citations, 8 of which are registered in WoS and 6 in SCOPUS.

Author: Ing. Stanislava Serečunová

Thesis title: Design, simulation and optimization of passive photonic devices
for communications and medical applications

Volume: 12 units

The dissertation thesis and its abstract are stored at the Faculty of Electrical Engineering and Information Technology of STU in Bratislava